Geochemistry of abyssal peridotites from the super slow-spreading Southwest Indian Ridge near 65°E: Implications for magma source and seawater alteration

ZHIGANG ZENG[1,*], QIAOYUN WANG[1], XIAOMEI WANG[1,2], SHUAI CHEN[1,2], XUEBO YIN[1] and ZHAOXUE LI[1]

[1]*Seafloor Hydrothermal Activity Laboratory of the Key Laboratory of Marine Geology and Environment, Institute of Oceanology, Chinese Academy of Sciences, Qingdao 266071, China.*
[2]*Graduate University of Chinese Academy of Sciences, Beijing 100049, China.*
[*]*Corresponding author. e-mail: zgzeng@ms.qdio.ac.cn*

The geochemical characteristics of abyssal peridotite samples from one dredge station (27°49.74′S, 65°02.14′E, water depth 4473 m) on the super slow-spreading Southwest Indian Ridge (SWIR) near 65°E were investigated. Abyssal peridotites recovered from this site were comprised mainly of lizardite, chlorite, carbonate and magnetite with minor amounts of talc, pyroxene phenocrysts and sparse olivines.

Serpentinites exhibit talc veins and major serpentine derived from serpentinization with relict olivine granuloblasts. Olivine grains in serpentinites display exsolution lamellae, indicating the occurrence of talc reduction or decompression during seawater–rock interaction. Pyroxene shows clear cleavage in two directions, with clinopyroxene or orthopyroxene exsolution lamellae. By contrast, bulk rock trace element patterns of serpentinites reveal depletion in most incompatible elements, similarly to the depleted mid-ocean ridge basalt mantle composition, indicating that the SWIR peridotites originated from a depleted mantle source magma and have experienced partial melting. Meanwhile, Rb, Ba, U, Pb, Sr, Li anomalies and the Ce/Pb ratio suggest that these serpentinites have been strongly altered by seawater.

1. Introduction

At present, it is generally accepted that mantle peridotites are widely exposed on the seafloor at slow-to-intermediate spreading ridges (e.g., Dick *et al.* 1984; Cannat *et al.* 1995). These peridotites have been interpreted to be the residues from variable degrees of partial melting related to the production of mid-ocean ridge basalts (e.g., Dick *et al.* 1984; Johnson *et al.* 1990), rather than being simple residues (Elthon 1992; Niu 1997; Niu and Hekinian 1997; Niu *et al.* 1997; Hellebrand *et al.* 2002; Brunelli *et al.* 2006; Seyler *et al.* 2007; Tamura *et al.* 2008; Godard *et al.* 2008). The peridotites are usually highly serpentinized, as a result of seawater–peridotite interaction, and are referred to in the literature as abyssal peridotites. In the serpentinite-hosted hydrothermal fields of slow-spreading mid-ocean ridges (Kelley *et al.* 2001; Douville *et al.* 2002; Fruh-Green *et al.* 2003), the abyssal peridotites still contain relics of mantle minerals, which contain primary information about melting and melt extraction processes beneath mid-ocean ridges. Hydrothermal interaction between peridotites or serpentinites and seawater is gaining increasing interest because of its importance in the rheology of the oceanic lithosphere (Escartin *et al.* 1997, 2001; Hirose *et al.*

Keywords. Abyssal peridotite; magma source; seawater alteration; Southwest Indian Ridge near 65°E.

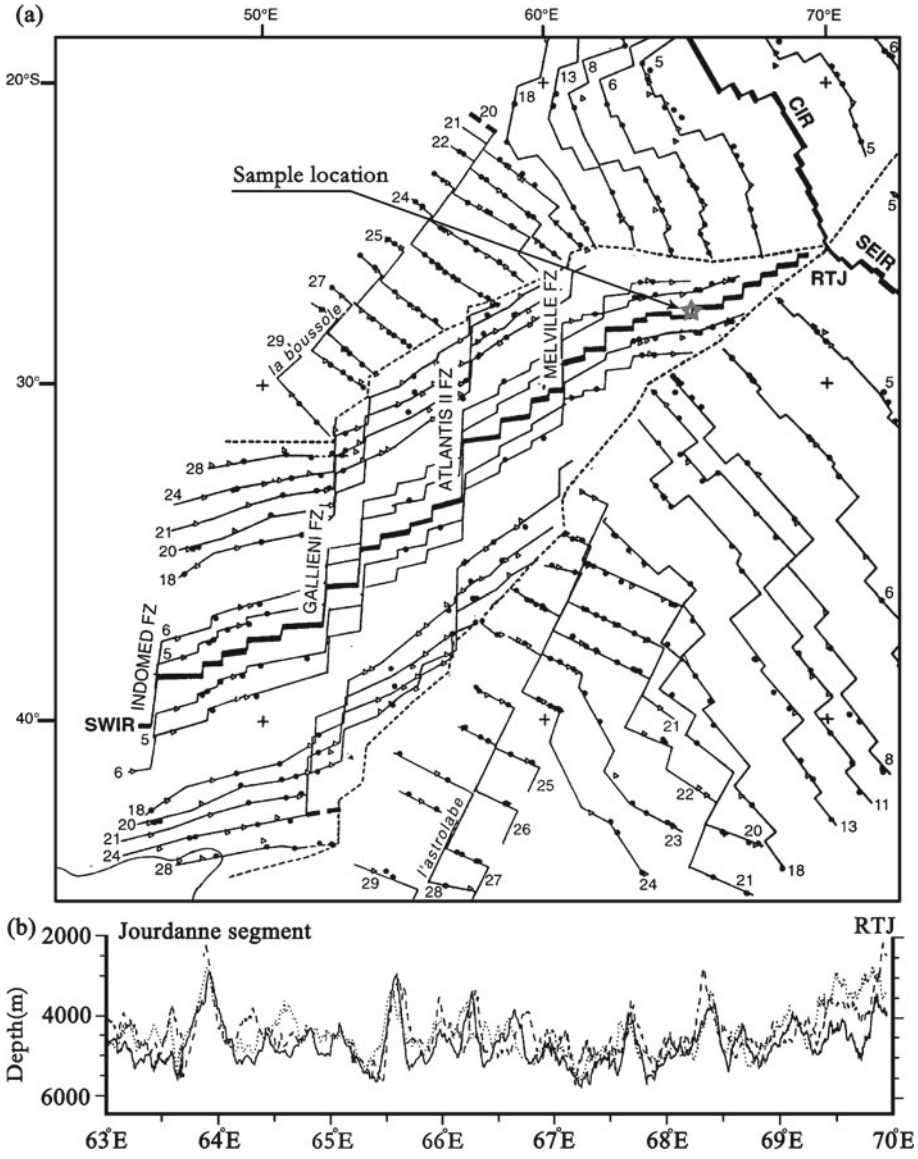

Figure 1. (**a**) Tectonic chart of the Southwest Indian Ocean (from Patriat *et al.* 1997). The dots are observed magnetic anomalies, the triangles are the rotated anomalies, and the dashed lines indicate the triple junction traces. Note that the SWIR axis was interpreted as a succession of short segments invariably linked by transform faults. (**b**) Depth variations along the axis and two parallel lines 5 km away from the axis (dotted for north and dashed for south) of the SWIR between 63°E and 70°E (after Patriat *et al.* 1997).

Table 1. *Major mineral assemblages of serpentinite samples from the super slow-spreading Southwest Indian Ridge near 65°E.*

Sample no.	Major mineral assemblages (%)
IR-D1-1-2	Lizardite (50%), pyroxene (25%), magnetite (10%)
IR-D1-3	Lizardite (40%), pyroxene (20%), magnetite (15%)
IR-D1-4	Magnesiohornblende (50%), chlorite (20%)
IR-D1-8-2	Lizardite (60%), chlorite (20%), magnetite (10%), pyroxene (5%), talc (2%)
IR-D1-9-2	Lizardite (20%), magnetite (12%), pyroxene (10%)
IR-D1-11-2	Lizardite (30%), carbonate (20%), magnesiohornblende (5%)

2006; Hilairet *et al.* 2008), geochemical budgets and/or sources for some elements in the oceans (Snow and Dick 1995; Niu 2004; Paulick *et al.* 2006), and microbial activities on and below the seafloor (Kelley *et al.* 2005a; Takai *et al.* 2006; Morishita *et al.* 2009).

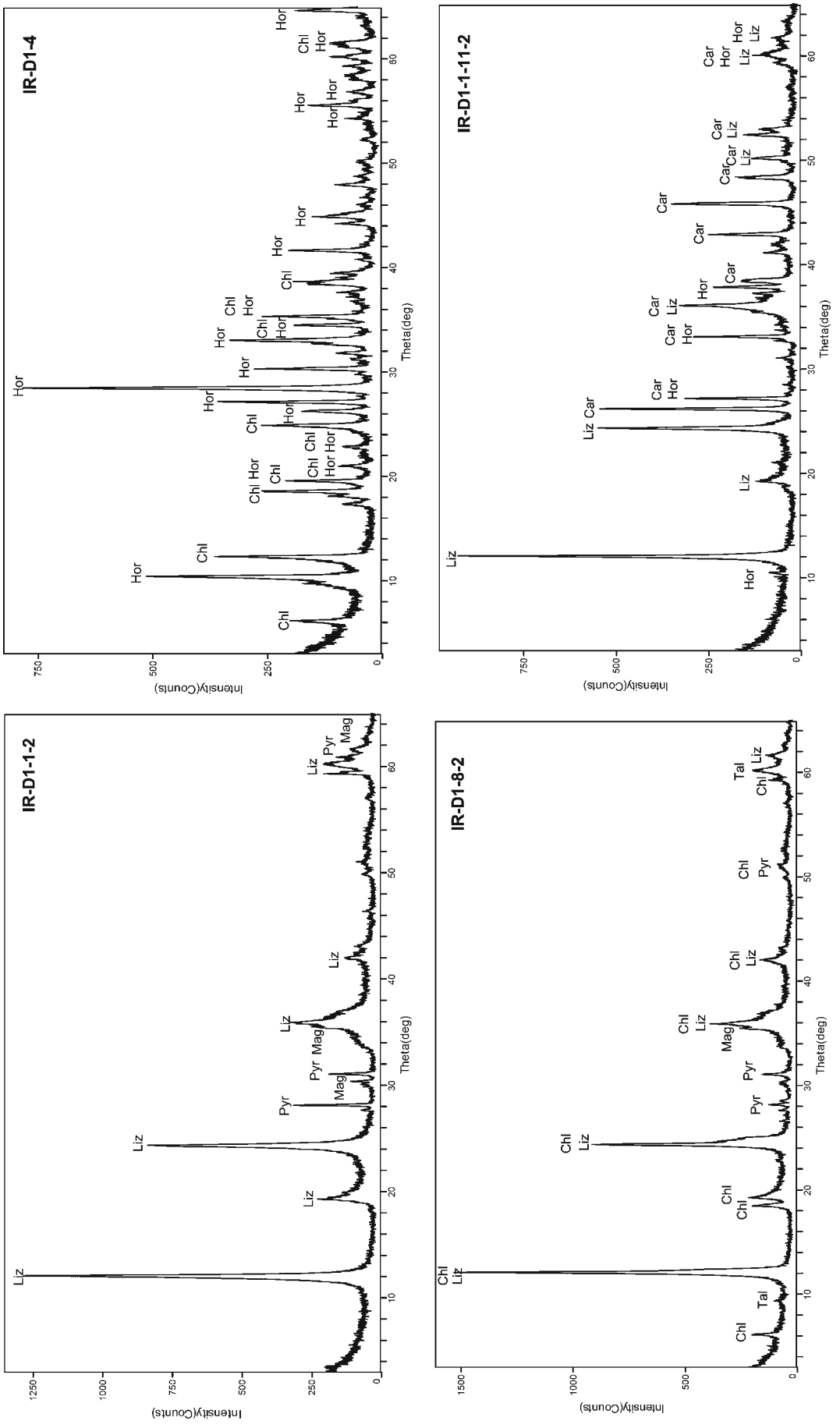

Figure 2. XRD profiles of bulk rock serpentinites from the SWIR near 65°E. Liz: Lizardite; Chl: Chlorite; Car: Carbonate; Tal: Talc; Pyr: Pyroxene; Mag: Magnetite; Hor: Mg-hornblend.

The Southwest Indian Ridge (SWIR), located within the region 45°∼70°E and 26°∼40°S, has been studied and investigated in terms of its morphology and geomagnetism by means of bathymetric techniques, and comparisons have been made with the Mid-Atlantic Ridge (MAR) (Mendel and Sauter 1997; Patriat *et al.* 1997). The SWIR is a typical super-slow spreading ridge, where the spreading rate is commonly considered to be less than 20 mm/a (Patriat and Parson 1989; Mendel

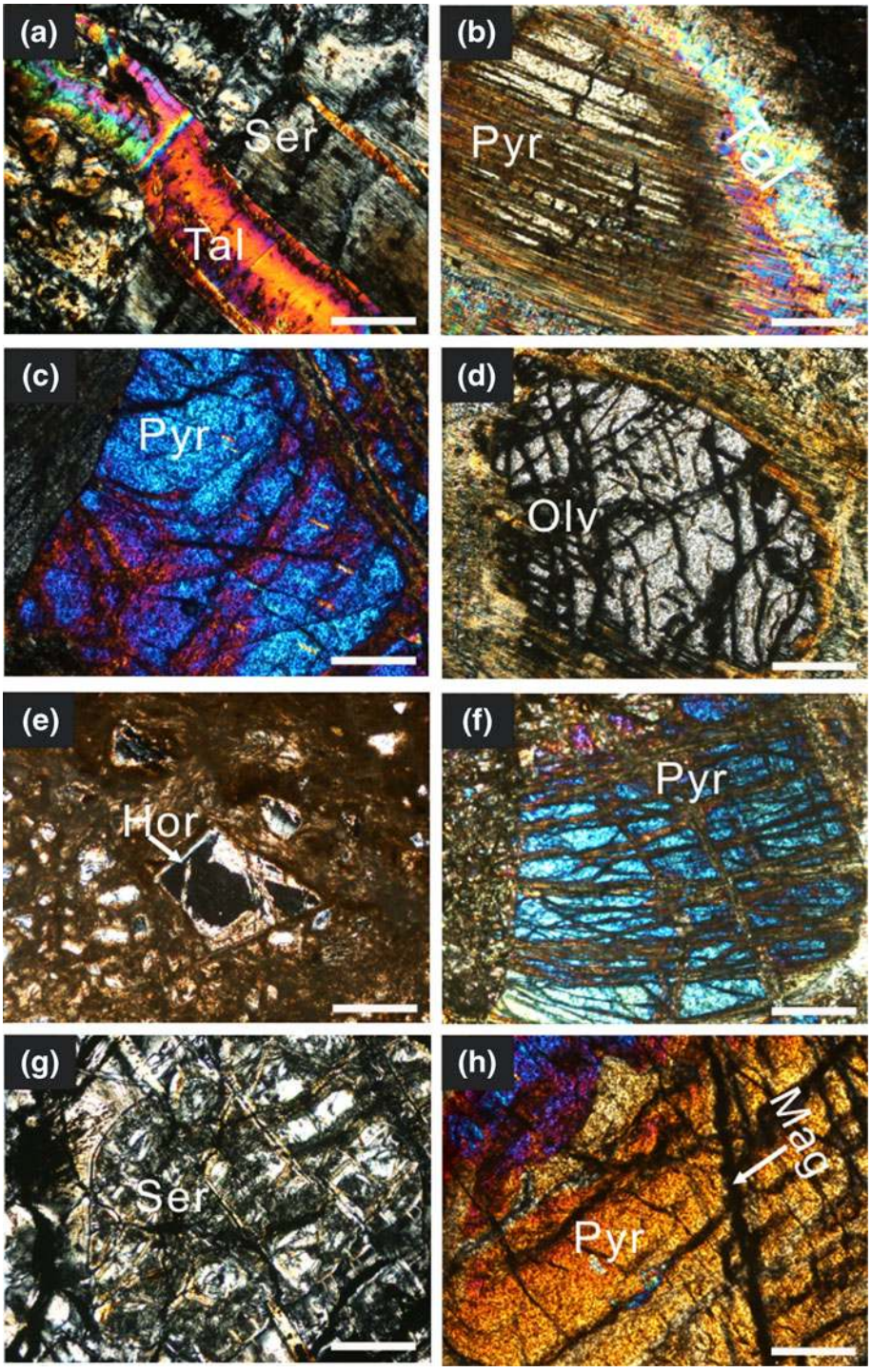

Figure 3. Photomicrographs of representative mineral structures. (**a**) Mineral assemblage: serpentine + talc, which are the resulting minerals from serpentinization; (**b**) pyroxene phenocrysts with exsolution lamellae; (**c**) a well-preserved pyroxene grain; (**d**) an olivine grain; (**e**) Mg-hornblend, the resulting mineral from seawater alteration; (**f**) a pyroxene granuloblast, showing the deformed cleavage; (**g**) mesh texture formed by serpentine; and (**h**) a magnetite vein cross-cutting the coarse pyroxene. Ser: Serpentine; Tal: Talc; Pyr: Pyroxene; Olv: Olivine; Hor: Mg-hornblend; Mag: Magnetite. Scale bars = 0.2 mm.

et al. 1997). Specifically, the spreading rate of the SWIR at 66°E, near the Melville fracture zone, has been measured to be 12.1 mm/a from magnetic anomaly reversals (White *et al.* 2001).

The formation mechanism and interaction between oceanic crust and mantle under the SWIR have been investigated in detail. Generally, the average thickness of the oceanic crust beneath the ridges at full spreading rates below 20 mm/a is around 6.3 ± 0.9 km (White *et al.* 1992; Bown and White 1994). However, due to the much lower densities of seamounts compared with MAR, magma production under the SWIR is attenuated compared with faster spreading oceanic ridges, leading to a slower magmatic supply to the ridge axis, cooler mantle temperatures and therefore lower degrees of partial melting (Cannat 1996; Mendel and Sauter 1997; Robinson *et al.* 2001; White *et al.* 2001; Cannat *et al.* 2006). Thus, some authors have suggested that about 10%–25% of the melt is trapped and solidified at depths of 10–20 km in the upper mantle under very slow-spreading ridges (Cannat 1996; White *et al.* 2001). In particular, Cannat *et al.* (2006) proposed an avolcanic, or nearly avolcanic mode of seafloor spreading which may be analogous to processes at the ocean-continent transition of continental margins (Whitmarsh *et al.* 2001), and which appears to have created nearly half of the oceanic crust in the SWIR.

Abyssal peridotite compositions can provide geochemical evidence, for the mantle source or processes such as slab subduction, metasomatism and seawater alteration. It has been inferred that such compositions are consistent with the combined histories of partial melting and subsequent melt migration, which cause either olivine addition or dissolution and precipitation reactions by equilibrium porous flow (Niu *et al.* 1997; Asimow 1999). On the other hand, the interaction between seawater and peridotite can transform olivine and pyroxene into serpentine minerals and other phyllosilicates (Bach *et al.* 2004; Paulick *et al.* 2006; Augustin *et al.* 2008), through several processes including the uptake of boron and sulfur by the serpentinization (Thompson and Melson 1970; Bonatti *et al.* 1984; Alt and Shanks 1998, 2003), generation of hydrogen and methane, which can be entrained into the hydrothermal plumes overlying peridotite outcrops (Charlou *et al.* 1998; Horita and Berndt 1999; Alt and Shanks 2003), and weathering of peridotite by cold seawater, which can also release significant Mg into the seawater (Snow and Dick 1995).

This study thoroughly investigated the geochemical characteristics of bulk rock compositions of the abyssal peridotites sampled at the super slow-spreading SWIR near 65°E. The overall goal of this study was to use observed alteration of the mineralogy and geochemistry to identify the characteristics of the magma source and to show new evidence for significant and characteristic changes in the bulk rock compositions associated with alteration in the super slow-spreading SWIR. Hence, this study contributes to the characterization of the geochemical budget of the lithosphere at super slow-spreading ridges. These results may have implications for our understanding of the formation processes of abyssal peridotites at mid-ocean ridges and of the interaction between abyssal peridotites and seawater.

2. Samples and methods

Some 19 abyssal peridotite samples were dredged from the super slow-spreading SWIR near 65°E (27°49.74′S, 65°02.14′E, water depth 4473 m) during the DY115-17A cruise (R/V DAYANG YIHAO, December 9, 2005) (figure 1). The retrieved peridotites exhibited evident serpentinization under the microscope, with a mineral assemblage of major lizardite, chlorite, carbonate and magnetite, plus minor amounts of talc and phenocrysts, as shown in table 1 and figure 2.

In addition to retaining the olivine particle morphology, the serpentine samples from the SWIR near 65°E also exhibited irregular particle shapes, for example, elongated strips, leaf-shapes and radial forms. Serpentine minerals were also observed with a mesh structure, hourglass structure, or in serpentine veins. Talc showed radial and vein-like forms, in veins up to 0.4 mm wide. Olivine mineral grains were mostly broken and surrounded by serpentine; some of these olivine grains are the residual particles of olivine minerals. Pyroxene particles can be transformed into talc, which then retains the original shape of the pyroxene. Some

Table 2. *Analytical precision and content range of major element compositions determined by XRF.*

Compositions	Content range (%)	Analytical precision (%)
SiO_2	15.0–95.0	±0.20
TiO_2	0.01–7.50	±0.005
Al_2O_3	0.20–25.0	±0.10
Fe_2O_3	0.20–25.0	±0.05
MnO	0.01–0.35	±0.005
MgO	0.20–40.0	±0.03
CaO	0.10–35.0	±0.03
Na_2O	0.10–7.50	±0.03
K_2O	0.05–7.50	±0.02
P_2O_5	0.01–1.00	±0.005

pyroxene minerals were wrapped in olivine and talc veins, occurring along with the exsolution lamellae, while some of the pyroxene grains were the residual particles of pyroxene minerals. Pyroxene showed clear cleavage in two directions, with clinopyroxene (Cpx) or orthopyroxene (Opx) exsolution lamellae (figure 3).

The compositions of these bulk rock samples were determined by X-ray diffraction (XRD) (D/MAX-2400) at the Institute of Geology

Table 3. *Bulk rock major element compositions of serpentinite samples and one standard rock (GSR-3) sample as determined by XRF (values in wt.%).*

Samples	SiO_2	TiO_2	Al_2O_3	Fe_2O_3	MnO	MgO	CaO	Na_2O	K_2O	P_2O_5	LOI	Total	MgO/ SiO_2	Mg#
Standard														
GSR-3	44.87	2.37	13.85	13.40	0.17	7.77	8.76	3.32	2.31	0.96	2.35	100.13	0.17	0.70
Group 1 (strongest serpentinized)														
IR-D1-2-1	53.81	0.03	0.43	7.86	0.14	23.53	9.34	0.03	0.02	0.01	4.84	100.03	0.44	0.92
IR-D1-2-2	43.19	0.06	3.42	6.64	0.07	33.02	2.38	0.13	0.03	0.01	10.91	99.86	0.76	0.95
IR-D1-2-3	42.32	0.05	2.07	7.29	0.11	34.73	0.82	0.14	0.05	0.02	12.27	99.86	0.82	0.95
IR-D1-4	53.01	0.04	2.54	5.08	0.08	24.82	9.54	0.08	0.01	0.01	4.98	100.19	0.47	0.95
IR-D1-11-1	26.20	0.02	0.75	6.49	0.09	25.98	17.05	0.01	0.01	0.02	22.78	99.39	0.99	0.94
IR-D1-11-2	24.30	0.03	0.84	5.67	0.07	23.77	19.89	0.04	0.01	0.02	24.55	99.18	0.98	0.94
IR-D1-11-2P	24.13	0.03	0.90	5.73	0.07	23.86	20.01	0.01	0.01	0.02	24.57	99.34	0.99	0.94
IR-D1-15	35.73	0.03	0.77	8.35	0.08	34.85	5.00	0.01	0.01	0.02	15.19	100.03	0.98	0.95
IR-D1-16-1	51.96	0.01	0.89	4.35	0.31	19.53	18.63	0.08	0.02	0.01	3.60	99.39	0.38	0.93
IR-D1-17-1	32.42	0.01	0.98	11.09	0.27	32.30	5.90	0.01	0.01	0.06	16.94	99.97	1.00	0.92
IR-D1-17-2	35.17	0.01	0.51	11.71	0.23	34.52	2.46	0.00	0.02	0.05	14.99	99.67	0.98	0.92
IR-D1-18-1	29.08	0.01	0.63	2.35	0.07	29.15	15.78	0.01	0.02	0.02	22.58	99.70	1.00	0.98
IR-D1-18-1P	28.95	0.01	0.62	2.36	0.07	29.27	15.85	0.01	0.01	0.02	22.60	99.77	1.01	0.98
IR-D1-18-2	32.56	0.02	0.55	6.36	0.26	33.28	8.37	0.01	0.01	0.02	17.91	99.35	1.02	0.95
IR-D1-18-3	33.82	0.02	0.76	8.49	0.07	36.44	3.88	0.01	0.01	0.01	16.24	99.74	1.08	0.94
Group 2 (medium serpentinized)														
IR-D1-5	44.89	0.04	5.53	5.92	0.07	29.40	5.30	0.00	0.01	0.01	8.83	100.00	0.65	0.95
IR-D1-6-1	39.17	0.06	2.14	7.26	0.09	37.30	0.79	0.01	0.01	0.01	12.87	99.70	0.95	0.95
IR-D1-6-2	38.89	0.06	2.14	8.08	0.09	36.95	0.83	0.01	0.01	0.01	12.64	99.71	0.95	0.95
IR-D1-6-2P	38.73	0.06	2.13	8.11	0.09	37.15	0.82	0.01	0.02	0.01	12.77	99.90	0.96	0.95
IR-D1-8-1	39.87	0.07	2.18	8.48	0.11	36.31	0.38	0.00	0.03	0.01	12.29	99.73	0.91	0.94
IR-D1-8-2	39.69	0.07	2.63	8.33	0.11	36.24	0.37	0.00	0.03	0.01	12.28	99.76	0.91	0.95
IR-D1-7-1	43.09	0.06	4.83	6.43	0.07	31.82	2.85	0.46	0.05	0.01	10.37	100.05	0.74	0.95
IR-D1-7-2	41.44	0.06	2.44	7.81	0.10	35.20	0.73	0.16	0.06	0.02	11.98	99.99	0.85	0.95
IR-D1-7-3	41.25	0.06	2.31	7.84	0.10	35.10	0.70	0.14	0.04	0.03	12.41	99.98	0.85	0.95
IR-D1-10-1	41.08	0.08	2.18	7.16	0.10	35.71	1.72	0.01	0.03	0.02	11.35	99.43	0.87	0.95
IR-D1-10-2	41.46	0.08	2.74	7.10	0.10	34.83	2.30	0.01	0.04	0.02	10.86	99.53	0.84	0.95
IR-D1-13-1	41.53	0.06	2.39	7.82	0.12	35.16	0.74	0.20	0.06	0.02	11.52	99.62	0.85	0.95
IR-D1-13-2	41.19	0.05	2.31	7.81	0.12	35.77	0.66	0.08	0.04	0.01	11.55	99.58	0.87	0.95
IR-D1-14	41.68	0.09	2.87	7.40	0.11	33.82	2.31	0.04	0.03	0.02	11.07	99.43	0.81	0.95
IR-D1-16-2	38.74	0.05	4.05	9.90	0.11	34.12	0.12	0.03	0.04	0.01	12.55	99.73	0.88	0.93
Group 3 (weakest serpentinized)														
IR-D1-1-1	38.30	0.06	1.89	7.89	0.10	37.20	0.51	0.01	0.02	0.02	13.44	99.44	0.97	0.95
IR-D1-1-2	38.74	0.06	1.89	8.06	0.09	37.05	0.61	0.01	0.01	0.02	12.93	99.46	0.96	0.95
IR-D1-3	40.53	0.06	1.79	8.49	0.09	36.35	1.40	0.01	0.01	0.02	11.43	100.18	0.90	0.94
IR-D1-9-1	41.07	0.02	1.41	7.56	0.10	36.16	0.12	0.10	0.04	0.02	13.19	99.80	0.88	0.95
IR-D1-9-2	42.15	0.02	1.32	7.37	0.10	35.71	0.53	0.05	0.02	0.02	12.32	99.62	0.85	0.95
IR-D1-12	39.95	0.07	1.65	7.06	0.10	37.48	0.05	0.01	0.01	0.00	12.99	99.37	0.94	0.96
IR-D1-19-1	38.84	0.05	1.85	9.82	0.10	35.86	0.12	0.01	0.02	0.03	13.16	99.87	0.92	0.94
IR-D1-19-2	40.57	0.05	1.65	7.59	0.09	37.56	0.40	0.01	0.02	0.02	11.91	99.88	0.93	0.95
PM	49.9	0.16	3.54			35.1	2.89	0.34	0.02					

Determined by the Institute of Geology and Geophysics, Chinese Academy of Sciences. PM, data from Taylor and McLennan (1985).

Table 4. *Analyses of standard reference materials by ICP-MS.*

	GBW07315		GBW07316		GBW07101		GBW07102		BHVO-2		BCR-2		DTS-2B	
	DV	RV	DV	RV	DV	RV	DV	RV	DV	RV	DV	RV	DV	RV
Li	48.0 ± 3.0	51 ± 3	31.3 ± 1.5	35 ± 2	0.63 ± 0.02	1.3 ± 0.5	1.86 ± 0.34	2.3 ± 0.4	4.75 ± 0.28	5	9.76 ± 0.44	9 ± 2	–	–
Sc	22.9 ± 0.5	23 ± 3	15.2 ± 0.2	15 ± 2	4.13 ± 0.13	4.9 ± 0.2	3.87 ± 0.16	4.8 ± 0.2	31.5 ± 0.7	32 ± 1	33.9 ± 0.6	33 ± 2	2.72 ± 0.04	3
V	97.3 ± 2.8	101 ± 8	71.9 ± 2.1	69 ± 6	34.3 ± 0.5	38.9 ± 5.6	15.7 ± 0.8	16.7 ± 5.6	–	–	–	–	17.6 ± 0.4	22 ± 8
Cr	57.3 ± 1.7	59 ± 6	38.3 ± 1	38 ± 5	–	–	2833 ± 20	2874 ± 68	–	–	–	–	13004 ± 105	15500 ± 1100
Co	74.9 ± 1.5	81 ± 8	53.3 ± 1.3	53 ± 4	82.6 ± 0.9	94.4 ± 7.9	90.4 ± 1.0	102 ± 7.9	43.5 ± 1.4	45 ± 3	37.2 ± 1.0	37 ± 3	115 ± 2	120 ± 10
Ni	155 ± 4.9	167 ± 12	107 ± 2.67	108 ± 9	2463 ± 16	2508 ± 79	2304 ± 18	2351 ± 783	114 ± 5	119 ± 7	–	–	3923 ± 65	3780 ± 220
Cu	346 ± 3.7	357 ± 20	229 ± 3.8	231 ± 10	2.09 ± 0.09	5.5 ± 0.8	5.26 ± 0.18	5.3 ± 0.3	136 ± 5	127 ± 7	24.6 ± 0.1	19 ± 2	2.91 ± 0.11	3
Zn	137 ± 2.9	137 ± 15	139 ± 2	142 ± 22	44.4 ± 0.6	45.4 ± 7.3	40.2 ± 0.05	43.6 ± 5.3	126 ± 4	103 ± 6	157 ± 4	127 ± 9	40.0 ± 1.1	45 ± 5
Ga	17.6 ± 0.3	18 ± 1	11.8 ± 0.1	12 ± 1	1.00 ± 0.02	1.2 ± 0.6	0.22 ± 0.01	0.38 ± 0.12	–	–	–	–	–	–
Rb	72.9 ± 2.0	73 ± 5	51.2 ± 0.6	50 ± 5	–	–	–	–	10.6 ± 0.6	9.8 ± 1.0	48.6 ± 1.0	48 ± 2	1.53 ± 0.04	3.5
Sr	281 ± 5.0	298 ± 23	652 ± 11	667 ± 68	1.56 ± 0.12	2.3 ± 0.6	34.3 ± 0.55	33.2 ± 6.2	375 ± 16	389 ± 23	330 ± 4	346 ± 14	–	–
Y	94.9 ± 1.2	98 ± 4	67.4 ± 0.4	69 ± 6	0.11 ± 0.02	0.14	0.10 ± 0.01	0.14	25.0 ± 1.3	26 ± 2	34.9 ± 0.4	37 ± 2	–	–
Zr	142 ± 3.1	140 ± 8	94.6 ± 1.0	94 ± 8	–	–	–	–	180 ± 6	172 ± 11	201 ± 4	188 ± 16	–	–
Nb	10.0 ± 0.3	11 ± 1	7.11 ± 0.18	6.9 ± 0.6	–	–	–	–	18.5 ± 0.62	–	–	–	–	–
Ba	2967 ± 30	3100 ± 300	2461 ± 42	2500 ± 200	5.67 ± 0.44	6.4 ± 2.8	11.5 ± 0.1	10.5 ± 3.3	125 ± 4	130 ± 13	670 ± 7	683 ± 28	10.5 ± 0.45	16
La	58.3 ± 1.2	62 ± 4	43.6 ± 0.5	44 ± 4	0.22 ± 0.01	0.19–0.25	0.19 ± 0.02	0.19 ± 0.24	15.9 ± 0.7	15 ± 1	26.4 ± 0.3	25 ± 1	–	–
Ce	76.9 ± 2.5	82 ± 6	53.9 ± 1.5	55 ± 4	0.39 ± 0.01	0.32–0.38	0.31 ± 0.01	0.4 ± 0.03	38.0 ± 1.2	38 ± 2	53.8 ± 0.8	53 ± 2	–	–
Pr	16.2 ± 0.6	17 ± 1	11.7 ± 0.3	12 ± 1	0.05 ± 0.01	0.045	0.040 ± 0.05	0.047	–	–	6.85 ± 0.15	6.8 ± 0.3	–	–
Nd	69.4 ± 0.9	75 ± 4	49.7 ± 1.3	51 ± 2	0.17 ± 0.02	0.15–0.18	0.176 ± 0.01	0.17–0.21	24.5 ± 0.8	25 ± 1.8	28.9 ± 0.9	28 ± 2	–	–
Sm	16.6 ± 0.3	18 ± 1	11.7 ± 0.1	12 ± 1	0.022 ± 0.002	0.021–0.033	0.027 ± 0.01	0.027–0.029	6.05 ± 0.21	6.2 ± 0.4	6.75 ± 0.17	6.7 ± 0.3	–	–
Eu	4.24 ± 0.06	4.5 ± 0.3	2.93 ± 0.06	3 ± 0.2	0.0055 ± 0.0005	0.004–0.063	0.0055 ± 0.0005	0.0057–0.008	–	–	–	–	–	–
Gd	16.6 ± 0.5	18 ± 1	11.8 ± 0.1	12 ± 1	0.024 ± 0.01	0.021–0.028	0.025 ± 0.006	0.026–0.033	5.80 ± 0.18	6.3 ± 0.2	6.60 ± 0.25	6.8 ± 0.3	–	–
Tb	2.9 ± 0.1	3.1 ± 0.3	2.01 ± 0.04	2 ± 0.2	0.030 ± 0.005	0.025–0.0045	0.030 ± 0.004	0.029–0.032	0.98 ± 0.03	0.9	1.12 ± 0.04	1.070 ± 0.040	–	–
Dy	15.7 ± 0.3	17 ± 1	11.0 ± 0.3	11 ± 1	0.020 ± 0.007	0.019–0.031	0.014 ± 0.006	0.020–0.033	–	–	–	–	–	–
Ho	3.37 ± 0.10	3.6 ± 0.2	2.36 ± 0.04	2.4 ± 0.2	0.005 ± 0.001	0.0046–0.0074	0.005 ± 0.001	0.004–0.0067	1.00 ± 0.04	1.04 ± 0.4	1.35 ± 0.04	1.330 ± 0.060	–	–
Er	8.93 ± 0.28	9.8 ± 0.7	6.15 ± 0.14	6.3 ± 0.2	0.02 ± 0.005	0.014	–	–	–	–	–	–	–	–
Tm	1.38 ± 0.04	1.4 ± 0.1	0.93 ± 0.03	0.960 ± 0.09	0.0035 ± 0.0005	0.0026–0.0041	0.0025 ± 0.0003	0.0028	–	–	0.56 ± 0.02	0.54	–	–
Yb	8.51 ± 0.43	8.9 ± 0.5	5.63 ± 0.09	5.8 ± 0.4	0.019 ± 0.005	0.019–0.022	0.011 ± 0.003	0.01–0.013	1.98 ± 0.10	2.0 ± 0.2	3.47 ± 0.11	3.5 ± 0.2	–	–
Lu	1.30 ± 0.03	1.3 ± 0.1	0.86 ± 0.04	0.89 ± 0.07	0.004 ± 0.001	0.003–0.005	0.0020 ± 0.0007	0.0019–0.0028	0.28 ± 0.02	0.28 ± 0.01	0.51 ± 0.01	0.51 ± 0.02	–	–
Hf	3.47 ± 0.09	3.6 ± 0.4	2.26 ± 0.07	2.3 ± 0.2	–	–	–	–	4.53 ± 0.29	4.1 ± 0.3	5.11 ± 0.08	4.8 ± 0.2	–	–
Ta	0.59 ± 0.01	0.6	0.40 ± 0.02	0.41	–	–	–	–	1.04 ± 0.04	1.4	–	–	–	–
Pb	42.7 ± 0.7	37 ± 4	20.8 ± 0.4	22 ± 5	2.50 ± 0.01	2.8 ± 0.3	2.54 ± 0.04	3.2 ± 0.8	–	–	11.1 ± 0.2	11 ± 2	–	–
Th	10.8 ± 0.1	11 ± 1	6.91 ± 0.14	7.0 ± 0.6	–	–	–	–	1.25 ± 0.05	1.2 ± 0.3	6.15 ± 0.25	6.2 ± 0.7	–	–
U	1.62 ± 0.03	1.9 ± 0.5	1.07 ± 0.03	1.1 ± 0.3	–	–	–	–	–	–	1.73 ± 0.08	1.69 ± 0.19	–	–

DV: Determined value; RV: Recommended value; "–" means no value.

and Geophysics, Chinese Academy of Sciences (IGGCAS). Bulk rock samples were powdered and pressed into tablets ready for measurement. A D/MAX-2400 instrument was operated at a voltage of 40 kV, with a current of 60 mA, a scan range of 3–65°2θ, a scan step of 0.02, and a scan velocity of 8°/min. Bulk rock major element compositions were analyzed on fused glass disks employing an Axios X-ray Fluorescence Spectrometer (XRF) at IGGCAS. All major element percentages were converted to oxide percentages. Analytical precision was based on certified standards and duplicate analyses are expressed in terms of relative percentages, which range from ±0.005% to ±0.20% (table 2). Samples of 5 g were used for determination of loss on ignition (LOI) by weighing after 1.5 h of heating at 1000°C (table 3).

For trace element analyses, 40 mg powders of each sample were dissolved in Teflon beakers by 2 ml HF, 0.6 ml HNO_3 and 0.25 ml $HClO_4$ at a temperature of 150°C. After heating for about 72 hours, the samples were dried at 150°C, and the residue was redissolved by 1 ml of HNO_3 and 1 ml of ultrapure H_2O (18.2 MΩ). The solutions were cooled and diluted by ultrapure H_2O (18.2 MΩ) to 1000 times and then analysed for trace elements

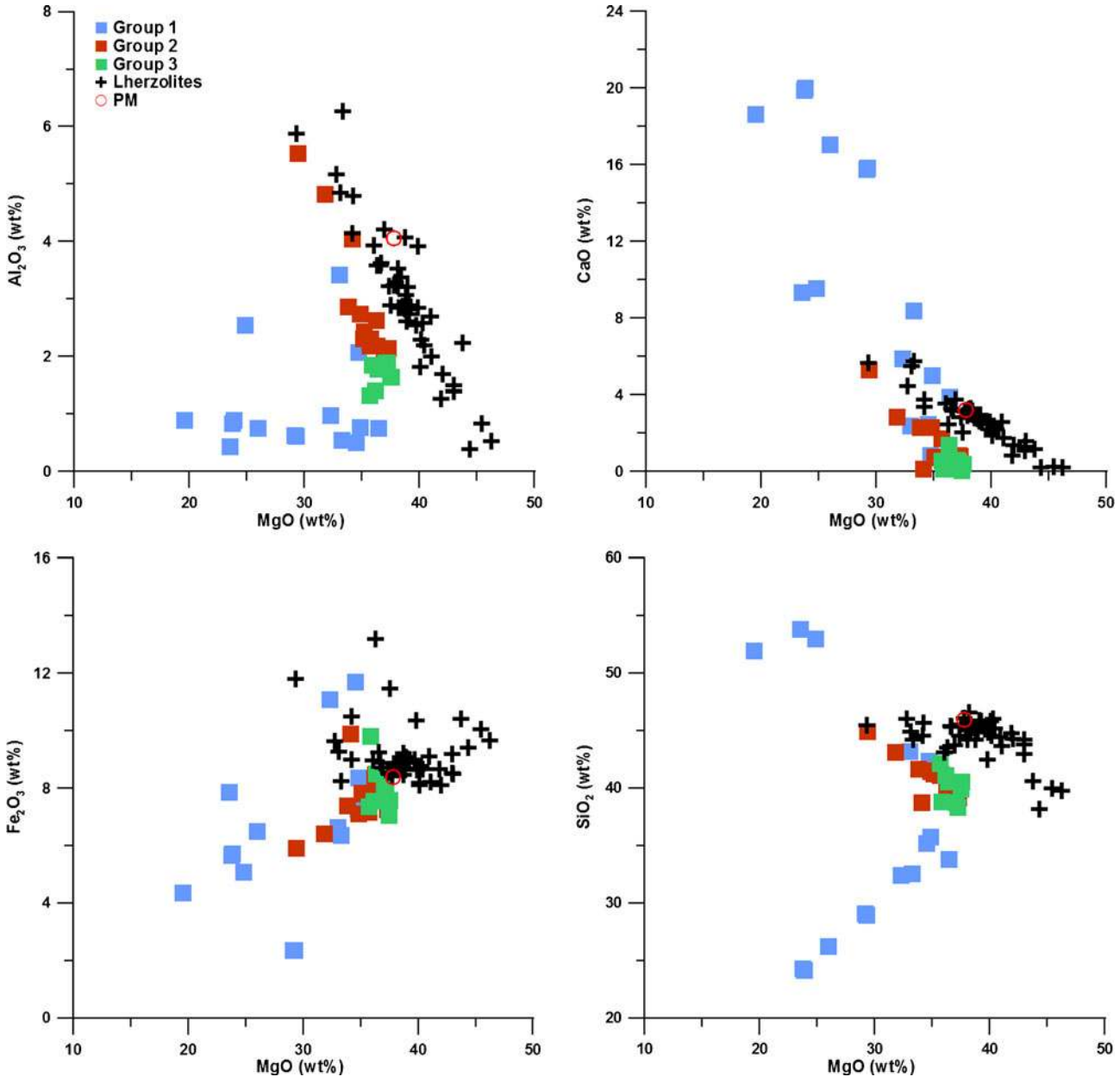

Figure 4. Bulk rock abundances of MgO *vs.* Al_2O_3, CaO, Fe_2O_3 and SiO_2 in the serpentinites. Data for primordial mantle (PM) and typical residual lherzolites of orogenic peridotites (cross symbol) are from Hofmann (1988), Bodinier (1988) and Bodinier *et al.* (1988), respectively.

Table 5. *Bulk rock trace element concentrations of serpentinite samples determined by ICP-MS.*

Samples	Li	Sc	V	Cr	Co	Ni	Cu	Zn	Ga	Rb	Sr	Zr	Nb	Ba	Hf	Ta	Pb	Th	U
Group 1 (strongest serpentinized)																			
IR-D1-2-1	7.29	2.52	20.9	134	30.8	346	20.6	56.2	1.07	1.60	6.38	3.63	0.11	1.06	0.04	0.01	1.12	0.02	0.41
IR-D1-2-2	19.4	8.61	61.6	4564	55.2	1638	2.19	60.7	5.81	1.63	5.14	1.01	0.10	1.69	0.04	0.01	0.99	0.01	0.34
IR-D1-2-3	25.8	9.25	61.0	4698	86.3	1502	26.4	83.6	3.86	1.68	9.22	1.77	0.06	4.79	0.04	0.02	1.20	0.02	0.88
IR-D1-4	1.85	7.02	41.0	3424	57.7	1657	3.17	69.8	3.03	1.47	4.15	0.48	0.03	0.55	0.03	0.02	1.02	–	0.26
IR-D1-11-1	2.36	3.94	27.0	3682	63.6	2027	3.06	31.2	0.96	1.58	2379	1.32	0.08	12.1	0.03	–	1.33	–	0.77
IR-D1-11-1P	2.35	4.22	28.3	3901	67.2	2130	3.61	33.2	1.03	1.57	2509	1.44	0.09	13.9	0.04	0.01	1.35	–	0.81
IR-D1-11-2	2.29	5.19	30.1	3366	40.3	1848	2.96	29.8	0.94	1.61	2752	1.70	0.10	8.76	0.04	–	0.95	–	0.71
IR-D1-15	1.57	4.92	30.7	749	91.0	2127	3.40	43.7	0.85	1.56	574	0.38	0.05	2.01	0.02	–	1.04	0.02	0.72
IR-D1-16-1	2.18	–	12.4	200	10.2	113	–	32.1	0.97	1.77	95.9	0.10	0.03	2.59	–	–	1.25	–	0.79
IR-D1-17-1	2.80	3.45	55.4	4568	102	2141	2.53	56.5	1.37	1.53	820	0.10	0.02	7.24	–	–	1.02	–	1.07
IR-D1-17-2	2.98	4.34	46.5	941	122	2519	1.37	54.2	0.80	1.50	402	0.12	0.02	6.79	–	–	1.01	–	1.04
IR-D1-18-1	0.78	2.45	18.0	395	48.0	1882	5.38	16.0	0.83	1.67	2074	0.41	0.04	14.3	0.01	–	1.54	–	1.18
IR-D1-18-2	0.30	5.53	28.6	6592	87.9	2212	18.5	67.1	0.74	1.48	1242	0.20	0.03	5.13	–	–	1.01	–	1.08
IR-D1-18-3	0.30	4.94	29.0	5889	97.0	2182	7.85	34.9	0.95	1.62	619	0.18	0.02	2.78	0.01	–	0.99	–	1.29
Group 2 (medium serpentinized)																			
IR-D1-5	7.33	7.43	43.2	3586	64.2	1465	0.53	40.1	8.12	1.54	12.2	0.65	0.02	3.22	0.04	0.02	1.22	–	2.62
IR-D1-6-1	1.92	14.5	65.0	4666	83.8	2224	27.7	36.5	2.14	1.50	3.70	0.64	0.01	1.63	0.05	0.01	1.11	–	0.84
IR-D1-6-2	1.92	12.6	58.7	4672	82.2	2128	23.1	38.6	2.12	1.50	2.80	0.54	0.02	1.69	0.04	0.02	1.04	–	0.82
IR-D1-6-2P	2.29	13.1	61.4	4753	84.2	2183	23.9	39.7	2.20	1.51	2.99	0.54	0.01	2.11	0.04	0.01	1.10	–	0.84
IR-D1-8-1	8.27	11.0	66.0	4575	84.7	1875	19.6	66.8	2.19	1.56	4.56	1.58	0.02	3.29	0.05	0.01	1.10	–	0.26
IR-D1-8-2	9.27	12.0	69.4	4979	88.0	1963	12.9	53.0	2.48	1.61	3.68	0.92	0.02	2.45	0.07	0.01	1.11	–	0.21
IR-D1-7-1	24.7	8.99	76.5	4385	49.8	1402	22.7	71.8	6.56	1.97	6.05	7.63	0.20	11.9	0.13	0.02	1.95	0.06	0.38
IR-D1-7-2	17.4	7.69	61.1	4482	81.8	1563	13.4	48.9	2.84	1.62	7.13	0.75	0.07	5.66	0.04	0.02	1.04	0.02	0.61
IR-D1-7-3	20.4	9.03	67.3	4622	77.5	1712	48.2	95.3	3.20	1.68	8.06	4.32	0.08	4.35	0.06	0.01	1.32	0.01	0.63
IR-D1-10-1	2.89	11.7	75.8	5566	73.6	1913	12.1	50.1	2.35	1.71	10.2	1.00	0.01	7.20	0.07	–	1.28	–	0.48
IR-D1-10-2	4.73	12.0	71.8	4926	82.3	1922	24.4	47.9	2.33	2.14	10.8	1.94	0.06	11.6	0.09	0.01	1.63	0.01	0.43
IR-D1-13-1	23.6	10.3	64.6	5276	78.1	2040	38.2	85.8	2.66	1.92	8.84	2.74	0.03	9.86	0.05	–	1.53	–	0.49
IR-D1-13-2	16.2	9.93	57.4	5365	81.8	1712	17.2	45.9	2.19	1.73	6.49	0.72	0.01	8.94	0.04	–	1.32	–	0.21
IR-D1-14	6.17	14.1	75.2	5807	83.4	1933	19.2	47.5	2.44	1.63	56.4	1.09	0.02	5.86	0.07	–	1.32	–	0.81
IR-D1-16-2	3.44	7.17	48.1	7564	126	2262	39.8	70.0	9.64	1.86	6.16	0.84	0.02	8.69	0.03	–	2.31	–	1.17

Table 5. *(Continued)*

Samples	Li	Sc	V	Cr	Co	Ni	Cu	Zn	Ga	Rb	Sr	Zr	Nb	Ba	Hf	Ta	Pb	Th	U
Group 3 (weakest serpentinized)																			
IR-D1-1-1	2.65	14.1	65.4	4378	82.3	2138	35.2	37.0	1.83	1.61	2.90	1.02	0.03	5.49	0.04	0.01	1.40	0.01	0.86
IR-D1-1-2	2.86	14.2	65.4	4703	82.0	1891	29.1	38.1	1.89	1.59	3.00	0.83	0.03	1.64	0.04	0.01	1.00	0.01	0.88
IR-D1-3	3.76	9.79	55.7	4106	84.0	1943	12.2	40.2	1.86	1.51	3.34	0.81	0.02	1.74	0.05	0.04	1.07	0.01	0.80
IR-D1-9-1	11.4	6.88	47.8	7524	95.2	2247	89.4	52.2	1.77	1.72	6.36	0.69	0.09	10.8	0.02	0.01	1.89	0.01	1.11
IR-D1-9-2	10.1	6.86	46.7	5701	86.4	1941	87.2	43.5	1.55	1.78	6.20	0.38	0.09	3.88	0.01	0.01	1.22	–	0.61
IR-D1-12	0.37	16.4	69.4	6236	86.4	2285	35.4	41.4	1.60	1.55	5.60	1.44	0.02	4.37	0.06	–	1.23	–	0.06
IR-D1-19-1	3.32	7.29	56.8	6419	65.5	2010	18.1	55.2	1.61	1.68	12.6	0.88	0.03	5.73	0.03	–	1.21	–	0.86
IR-D1-19-2	2.25	7.65	48.7	5076	75.4	1749	18.0	43.2	1.53	1.95	6.85	0.59	0.01	3.00	0.03	–	1.10	–	0.49
IR-D1-19-2P	2.04	7.58	49.3	5169	75.6	1721	15.8	43.3	1.52	1.80	6.55	0.61	0.02	2.81	0.04	–	1.06	–	0.48

Determined by the Institute of Oceanology, Chinese Academy of Sciences. "–" means no value. All values are given in ppm.

by an Inductively Coupled Plasma Mass Spectrometer (ICP-MS) (ELAN DRC II, American PE Company) at the Institute of Oceanology, Chinese Academy of Sciences (IOCAS), Qingdao. GBW07315, GBW07316, GBW07101, GBW07102, DTS-2b, BCR-2 and BHVO-2 were used as reference materials for bulk rock analyses. Detection limits of the ICP-MS for rare earth elements (REE) and other trace elements were 10^{-8} g/g, and the analytical precisions (RSD, n = 3) of REE and other trace elements were <5%. Analyzed uncertainties (2σ) of ICP-MS data at the ppm level were better than ±10% for trace elements and REE. Analyses of standards were in agreement with the recommended values (table 4).

3. Results

3.1 *Bulk rock major element compositions*

Table 3 shows that all except four serpentinite samples had large LOI values, ranging from 10% to 24% and indicating a strong degree of serpentinization. Several serpentinite samples displayed extremely high CaO contents, from 5% to 20%, suggesting that the rock gained a high Ca content following reaction with seawater.

According to the bulk rock major element composition, these serpentinites from the SWIR can be divided into three groups (see table 3, figure 4). Group 1 is characterized by significantly higher CaO (by up to 20%), and by a much lower Al_2O_3 which varies from 0.43% to 3.42%, relative to primary mantle (PM) (CaO 2.89%, Al_2O_3 3.64%) (Taylor and McLennan 1985). Group 2 exhibits higher Al_2O_3 contents than PM and comparable CaO and SiO_2 to those of the abyssal peridotites from the Pacific and Indian Ocean Ridge-transform systems (CaO contents varying from 0.01% to 3.91%, avg. 1.30%, n = 122) (Niu 2004). Group 3 displays intermediate Al_2O_3 and lower SiO_2 compared with abyssal peridotites from the Pacific and Indian Ocean Ridge-transform systems (Niu 2004). Some of these serpentinites from the SWIR were close to the melting trend and preserved the higher MgO/SiO_2 ratios typical of mantle rocks ($MgO/SiO_2 > 1$). In contrast to these melt–rock interaction trends, serpentinites from the SWIR had MgO/SiO_2 ratios below those of the terrestrial range (0.4–1). Talc alteration of serpentinites at the SWIR caused a further decrease in MgO/SiO_2 ratios that was likely due to Si-metasomatism (Paulick *et al.* 2006).

3.2 *Trace element abundances of the bulk rock*

All trace element data used for this study are listed in table 5. Most serpentinite samples showed very

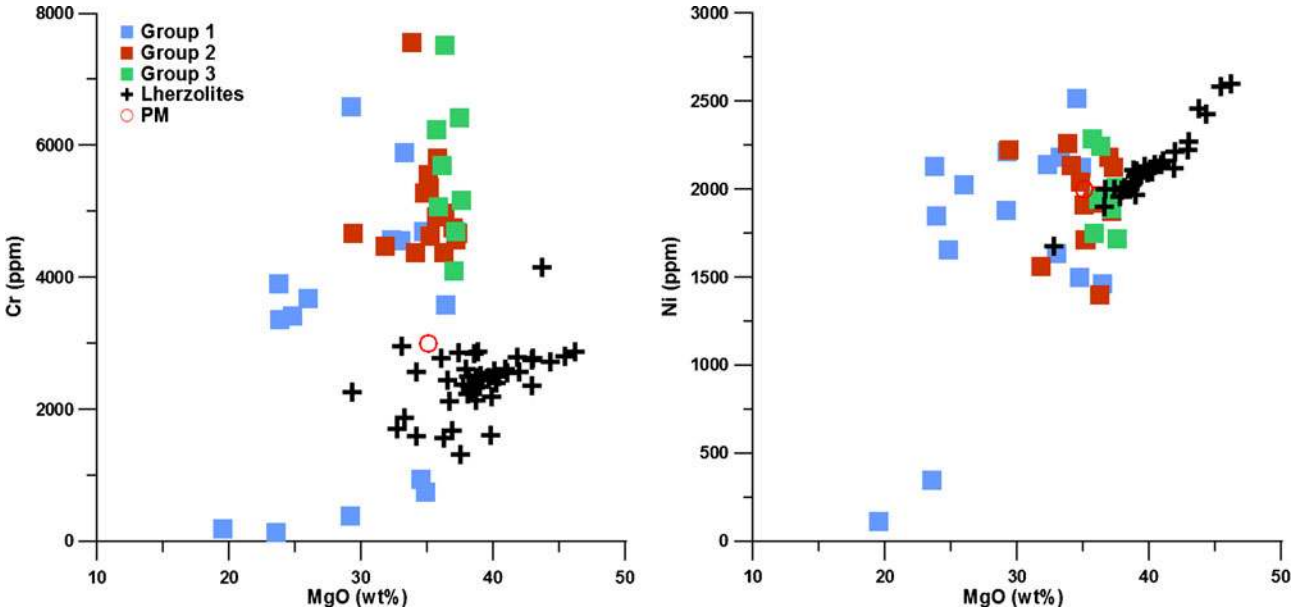

Figure 5. Bulk rock abundances of MgO *vs.* Cr and Ni in the serpentinites. Data for primordial mantle (PM) and typical residual lherzolites of orogenic peridotites (cross symbol) are from Taylor and McLennan (1985), Bodinier (1988) and Bodinier *et al.* (1988), respectively.

high Cu concentrations, of >3 ppm and up to 89.4 ppm. La and Eu contents varied markedly, up to 0.357 and 0.104 ppm, respectively. The samples showed much lower concentrations of Zr, Tb, Th and U and REEs. Serpentinites were enriched in Co, Ni, Cu, Zn, V and Sc, and contained comparable abundances of these enriched elements at levels comparable to PM (Co = 100 ppm, Ni = 2000 ppm, Cu = 28 ppm, Zn = 50 ppm, V = 128 ppm and Sc = 13 ppm) (Taylor and McLennan 1985).

Volatile or fluid-related elements, such as Rb, Ba, Li and Pb, together with Sr, in serpentinites displayed significantly higher abundances compared with those in PM, with some even close to the corresponding contents in seawater. Serpentinites also exhibited a distinctive depletion in Zr, Th and Nb.

The Cr concentrations of serpentinite samples were relatively high (up to 7564 ppm), which could be due to the presence of Cr-spinel. The Ni concentrations also showed a similar enrichment (up to 2285 ppm), and were higher than Ni contents (1300–1600 ppm) in lherzolite from the Central Indian Ridge (Engel and Fisher 1975). Zr and Y in the serpentinites from this study site had very low concentrations (<8 ppm). Among the trace elements, Cr and Ni correlated positively with MgO (figure 5).

All rare earth element data used for this study are listed in table 6. ΣREE of the serpentinites varied from 0.58 to 8.91 ppm. Most of the samples showed characteristic positive Eu anomalies (δEu up to +9.36). Figure 6 illustrates that the normalized REE patterns of the serpentinites were flat, except for the negative Ce anomalies, which is similar to the pattern in seawater, inferring serpentinites from the study site have experienced seawater alteration.

4. Discussion

4.1 *Petrological signatures and correlations in major element compositions*

Abyssal peridotites from the super slow-spreading SWIR near 65°E were predominantly intensely serpentinized. Serpentine formed mesh textures after olivine, cut by myriad small veinlets of serpentine ± magnetite. Serpentine minerals were mainly lizardite. The high abundances of lizardite indicate their formation at relatively low temperatures, around 130°C to 185°C (Wenner and Taylor 1973; Mével 2003; Ray *et al.* 2008). The serpentinization favoured formation of an extensive mesh texture, characterized by serpentine replacing olivine (figure 3g), with the abundant latter mineral forming magnetite strings cross-cutting the pyroxene (figure 3h). The distribution of magnetite in the serpentinite has often been correlated with a high degree of serpentinization (Ray *et al.* 2008). At advanced stages of serpentinization, the magnetite migrates out of the mesh or hourglass textural units into cross-cutting lenses, and the rock usually

Table 6. *Bulk rock rare earth element concentrations of serpentinite samples determined by ICP-MS.*

Samples	La	Ce	Pr	Nd	Sm	Eu	Gd	Tb	Dy	Ho	Er	Tm	Yb	Lu	Y
Group 1 (strongest serpentinized)															
IR-D1-2-1	0.181	0.549	0.129	0.748	0.304	0.052	0.323	0.069	0.458	0.091	0.287	0.050	0.331	0.047	2.37
IR-D1-2-2	0.238	0.716	0.113	0.626	0.187	0.064	0.220	0.044	0.319	0.072	0.217	0.036	0.225	0.033	1.88
IR-D1-2-3	0.229	0.399	0.073	0.351	0.108	0.037	0.145	0.027	0.207	0.048	0.153	0.029	0.160	0.028	1.29
IR-D1-4	0.115	0.033	0.047	0.139	0.056	0.022	0.087	0.022	0.166	0.040	0.138	0.023	0.134	0.021	1.10
IR-D1-11-1	0.248	0.475	0.111	0.465	0.128	0.042	0.141	0.018	0.151	0.031	0.093	0.015	0.085	0.013	0.87
IR-D1-11-1P	0.279	0.489	0.115	0.480	0.134	0.043	0.141	0.024	0.150	0.033	0.097	0.016	0.083	0.014	0.93
IR-D1-11-2	0.290	0.593	0.124	0.502	0.144	0.045	0.167	0.025	0.188	0.041	0.128	0.021	0.128	0.020	1.13
IR-D1-15	0.085	0.003	0.021	0.084	0.011	0.005	0.024	–	0.047	0.013	0.051	0.010	0.062	0.011	0.39
IR-D1-16-1	0.179	0.027	0.046	0.116	0.012	0.037	0.013	–	0.015	–	0.019	–	–	–	0.12
IR-D1-17-1	0.156	0.010	0.028	0.125	0.029	–	0.047	–	0.060	0.018	0.067	0.013	0.078	0.018	0.88
IR-D1-17-2	0.122	0.013	0.026	0.127	0.026	0.010	0.047	–	0.065	0.020	0.080	0.015	0.082	0.019	0.88
IR-D1-18-1	0.146	0.054	0.046	0.130	0.019	0.008	0.023	–	0.026	–	0.029	–	0.024	–	0.23
IR-D1-18-2	0.094	0.028	0.032	0.111	0.024	0.010	0.026	–	0.038	–	0.037	–	0.025	–	0.24
IR-D1-18-3	0.077	0.032	0.026	0.105	0.019	0.010	0.027	–	0.035	–	0.035	–	0.032	–	0.23
Group 2 (medium serpentinized)															
IR-D1-5	0.135	0.115	0.038	0.170	0.061	0.040	0.101	0.023	0.176	0.041	0.143	0.024	0.154	0.022	1.14
IRD1-6-1	0.052	0.043	0.026	0.174	0.081	0.029	0.124	0.028	0.221	0.054	0.187	0.031	0.199	0.030	1.38
IRD1-6-2	0.048	0.036	0.025	0.174	0.080	0.035	0.122	0.034	0.219	0.052	0.172	0.028	0.177	0.028	1.34
IRD1-6-2P	0.051	0.042	0.025	0.175	0.088	0.038	0.123	0.026	0.214	0.052	0.174	0.031	0.181	0.031	1.37
IR-D1-8-1	0.168	0.145	0.049	0.279	0.090	0.036	0.133	0.026	0.222	0.055	0.172	0.031	0.184	0.032	1.32
IR-D1-8-2	0.116	0.100	0.037	0.224	0.099	0.041	0.149	0.037	0.273	0.060	0.202	0.035	0.209	0.034	1.57
IR-D1-7-1	0.357	1.490	0.223	1.208	0.364	0.104	0.430	0.073	0.534	0.117	0.357	0.061	0.392	0.056	3.14
IR-D1-7-2	0.229	0.364	0.073	0.373	0.107	0.041	0.135	0.030	0.206	0.048	0.150	0.027	0.165	0.026	1.27
IR-D1-7-3	0.270	0.487	0.082	0.380	0.114	0.037	0.134	0.029	0.217	0.050	0.163	0.027	0.175	0.027	1.31
IR-D1-10-1	0.067	0.058	0.029	0.225	0.115	0.044	0.176	0.044	0.337	0.074	0.246	0.044	0.257	0.042	2.03
IR-D1-10-2	0.089	0.131	0.039	0.278	0.132	0.063	0.240	0.054	0.382	0.086	0.264	0.046	0.282	0.043	2.28
IR-D1-13-1	0.167	0.124	0.045	0.234	0.078	0.032	0.109	0.026	0.203	0.049	0.159	0.024	0.174	0.028	1.25
IR-D1-13-2	0.075	0.044	0.025	0.169	0.066	0.032	0.118	0.023	0.204	0.050	0.170	0.027	0.183	0.029	1.29
IR-D1-14	0.064	0.049	0.029	0.220	0.121	0.059	0.212	0.045	0.371	0.085	0.274	0.046	0.296	0.049	2.30
IR-D1-16-2	0.087	0.133	0.027	0.136	0.038	0.026	0.055	0.010	0.090	0.022	0.086	0.015	0.100	0.018	0.64

Table 6. *(Continued)*

Samples	La	Ce	Pr	Nd	Sm	Eu	Gd	Tb	Dy	Ho	Er	Tm	Yb	Lu	Y
Group 3 (weakest serpentinized)															
IR-D1-1-1	0.070	0.091	0.025	0.170	0.065	0.032	0.116	0.029	0.218	0.053	0.163	0.028	0.186	0.030	1.33
IR-D1-1-2	0.056	0.057	0.023	0.169	0.072	0.029	0.114	0.028	0.214	0.050	0.171	0.030	0.180	0.030	1.33
IR-D1-3	0.056	0.038	0.025	0.192	0.084	0.035	0.118	0.030	0.217	0.050	0.162	0.025	0.167	0.026	1.32
IR-D1-9-1	0.139	0.228	0.036	0.189	0.042	0.056	0.049	–	0.063	0.017	0.062	0.011	0.067	0.011	0.52
IR-D1-9-2	0.087	0.090	0.028	0.160	0.030	0.049	0.040	–	0.051	0.015	0.056	0.011	0.057	0.012	0.45
IR-D1-12	0.068	0.118	0.034	0.230	0.095	0.047	0.137	0.037	0.262	0.059	0.193	0.035	0.229	0.035	1.61
IR-D1-19-1	0.111	0.081	0.039	0.246	0.082	0.022	0.116	0.026	0.192	0.044	0.140	0.024	0.154	0.025	1.18
IR-D1-19-2	0.063	0.035	0.024	0.181	0.083	0.026	0.114	0.021	0.189	0.044	0.142	0.023	0.139	0.023	1.17
IR-D1-19-2P	0.060	0.038	0.024	0.179	0.072	0.026	0.113	0.018	0.184	0.042	0.137	0.024	0.154	0.023	1.13

Determined by the Institute of Oceanology, Chinese Academy of Sciences. "–" means no value. All values are given in ppm.

appears as green or often pale green (Wicks and Whittaker 1977; Ray *et al.* 2008).

Seawater–peridotite reaction can significantly alter the mineral assemblage of peridotite, leading to the production of serpentine ± magnetite ± talc in serpentinites (Hajash and Chandler 1981; Janecky and Seyfried 1986). The abyssal peridotites from the SWIR near 65°E were significantly altered, with substantial amounts of olivine, relatively minor amounts of dissolved pyroxene, and alteration products that included lizardite, talc, chlorite and carbonate.

Most serpentinites from the SWIR near 65°E were relatively low in SiO_2 and Fe_2O_3 compared with abyssal peridotites from the Pacific and Indian Ocean Ridge-transform systems (SiO_2 contents varying from 39.13% to 48.72%, mean 45.71%, n=125; FeO_{tot} contents varying from 6.46% to 12.12%, mean 8.53%, n=125) (Niu 2004), with SiO_2 and Fe_2O_3 contents variably ranging from 24% to 53% and 2% to 11%, respectively. MgO contents, varying from 19% to 37%, were also lower than those in abyssal peridotites from the Pacific and Indian Ocean Ridge-transform systems (from 36.26% to 46.29%, mean 41.93%, n = 125) (Niu 2004). However, serpentinites showed a significantly high Mg#, in the range 92–98, suggesting that either Mg enrichment and Fe depletion occurred during serpentinization of peridotites, or that seawater alteration resulted in Fe loss.

Generally, the major element composition of bulk rock in depleted mantle peridotites shows striking correlations, for example, increasing FeO_{tot}, Ni, Co, and decreasing Al_2O_3, SiO_2, CaO, Sc, Cr, Yb_N, with increasing MgO. In particular, the MgO∼FeO_{tot} and MgO∼SiO_2 correlations were similar to those identified in abyssal peridotites (Niu *et al.* 1997; Rampone *et al.* 2004). The serpentinites displayed consistent correlations of Al_2O_3, CaO, Fe_2O_3 and SiO_2 with MgO (figure 4). However, one distinct observation of these serpentinites from the SWIR near 65°E is that Groups 1 and 3 showed positive correlation between SiO_2 and MgO. The observed positive correlation between SiO_2 and MgO, and the negative correlation between SiO_2 and increasing loss on ignition (LOI) in the serpentinites from the SWIR near 65°E (figure 7), is similar to the corresponding characteristics of peridotites from the Izu-Bonin-Mariana forearc and serpentinite muds from the Mariana forearc (Parkinson *et al.* 1992; Savov *et al.* 2005); in addition, the high LOI values of serpentinite samples are consistent with the high degrees of serpentinization (Boschi *et al.* 2008), suggesting that the degree of serpentinization is likely to have affected the major element concentrations in the serpentinites.

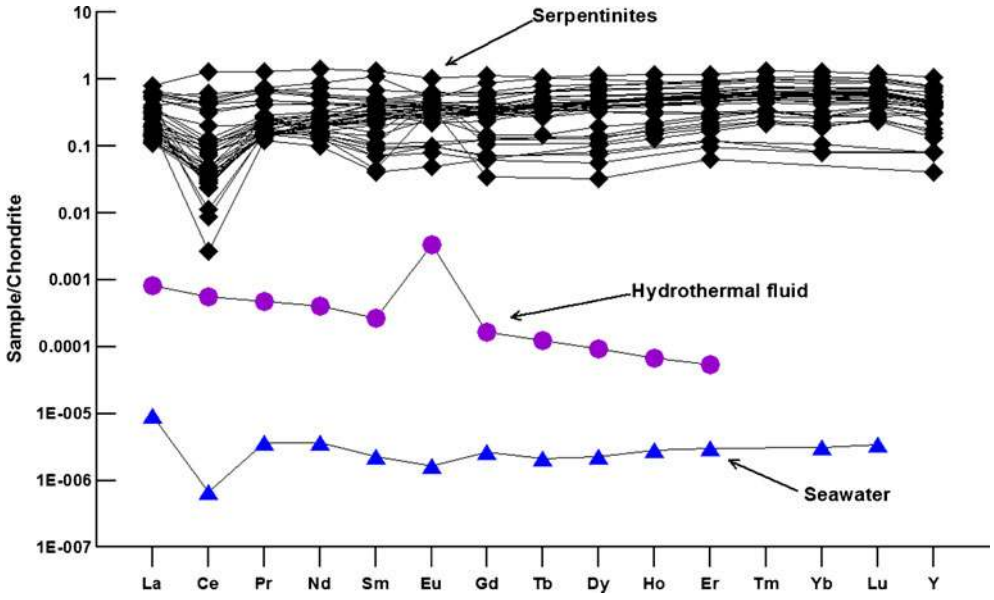

Figure 6. Chondrite-normalized REE patterns of serpentinites (chondrite REE data from McDonough and Sun 1995). Seawater and hydrothermal fluid data are from Turekian (1968) and Klinkhammer *et al.* (1994), respectively.

4.2 *Partial melting*

The dominant source of peridotite appears to be the upper mantle, based on mineralogical and chemical characteristics (Engel and Fisher 1975; Prinz *et al.* 1976), and on seismic and magnetic investigation of oceanic crust (Aumento and Loubat 1971; Christensen 1972; Fox *et al.* 1976).

Abyssal peridotites, which are extensively altered pieces of oceanic mantle that have been sampled from each of the major ridge systems in the ocean basins (Hamlyn and Bonatti 1980; Dick *et al.* 1984), may retain information on both the original partial melting process and concurrent or later interactions with partial melts from other sources (Baker and Beckett 1999).

Bulk rock $A1_2O_3$ contents of Groups 2 and 3 in serpentinites from the super slow-spreading SWIR near 65°E all decreased with increasing MgO (figure 4), while Fe_2O_3–MgO trends were essentially horizontal. Bulk rock CaO content was negatively correlated with MgO, while the bulk

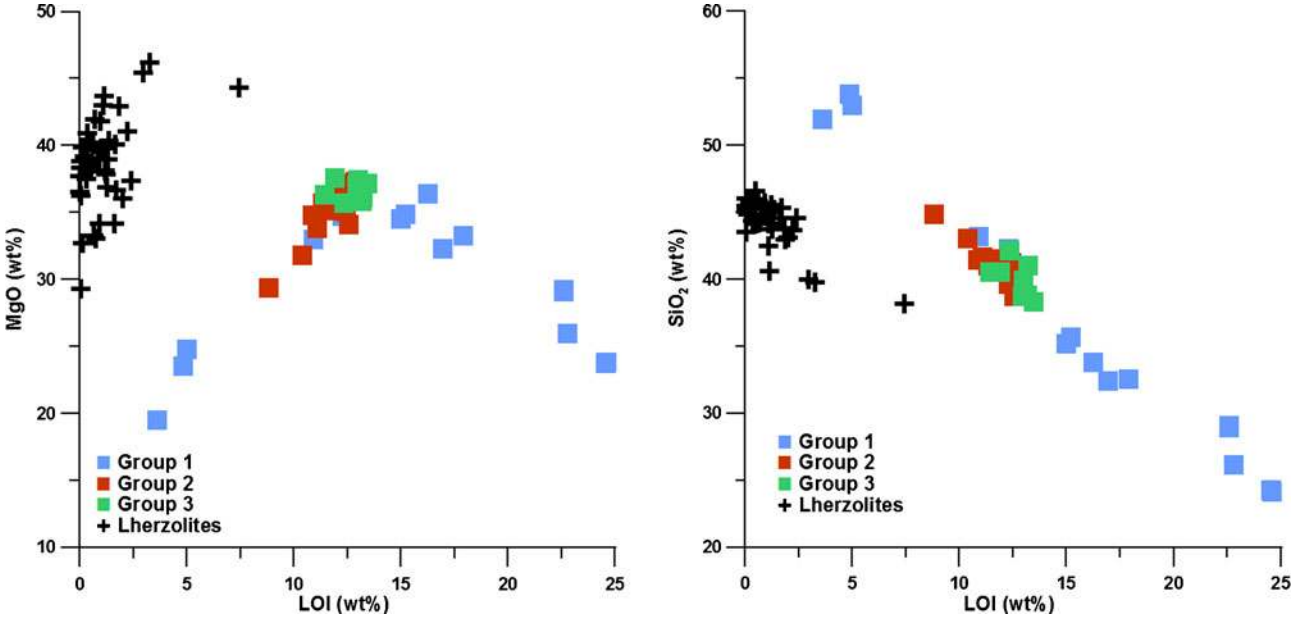

Figure 7. Bulk rock abundances of LOI *vs.* SiO_2 in the serpentinites. Data on the typical residual lherzolites of orogenic peridotites (cross symbol) are from Bodinier (1988) and Bodinier *et al.* (1988), respectively.

rock Ni–MgO contents were positively correlated, with both trends being linear (figure 5). All of these relationships are qualitatively consistent with those expected for high pressure partial melting of peridotites (Baker and Stolper 1994; Walter 1998).

Bulk rock trace elements in serpentinites from the super slow-spreading SWIR near 65°E were normalized by corresponding PM values and are plotted in figure 8. In the PM-normalised multi-element plot, the present serpentinites display enrichment of the large ion lithophile elements (LILEs; e.g., Sr, K, Ba, U, Th) and depletion of the HFSEs (e.g., Ti, Zr, Nb, Hf) and REE. In addition, most incompatible elements in all of the serpentinites were depleted to a greater extent than those of depleted mid-ocean ridge basalt mantle compositions (DMM), indicating that the serpentinites originated from the depleted mantle source magma and have experienced partial melting.

Chondrite-normalized REE patterns of serpentinites are plotted in figure 6. The relatively depleted LREE pattern of serpentinites indicates the occurrence of partial melting, and the negative Ce anomaly could result from the peridotite–seawater interaction (Luo *et al.* 2004; Class and le Roex 2008).

Bulk rock MgO values of abyssal peridotites still retain some magmatic signals, such as the extent of melting or melt depletion, and although abyssal peridotites have undoubtedly experienced some MgO loss and probably other changes, the original melting systematics remain largely preserved in serpentinites (Niu 2004). Figure 9 shows the relationship between indicative trace elements and major element composition. As the partial melting proceeds, Al_2O_3, Yb, Ce and Zr decrease with increasing MgO. The arrows in figure 9 explicitly illustrate the directions of partial melting and the variations of Yb, Ce and Zr in serpentinites. Therefore, it is inferred that serpentinites in the samples have experienced partial melting.

4.3 *Seawater–rock interactions*

Seawater alteration of abyssal peridotites is a complicated process, involving both serpentinization (∼<250°–500°C) and weathering (∼2°–3°C), and can take place under a range of temperatures and redox conditions during the different stages (Snow and Dick 1995; Bach *et al.* 2004). The intensity of serpentinization is mirrored by the LOI, as LOI values clearly covary with the degree of serpentinization (Harvey *et al.* 2006). The high LOI values (mostly 10–13 wt%) of these samples show that they are all hydrated (Pereira *et al.* 2003) and have consistently high to very high degrees of serpentinization (Boschi *et al.* 2008). Bulk rock major elements of the serpentinite samples have lower MgO contents compared with those of the fresh peridotites, and the Mg loss may be attributed to the replacement of serpentine by talc (Bach *et al.* 2004). It is possible that the apparent Mg loss in analyzed serpentinite samples has resulted from the seafloor weathering of serpentine (Niu 2004), reflecting the loss of Mg during seawater alteration of abyssal peridotites on the seafloor (Snow and Dick 1995). These samples also have higher contents of CaO than those of the fresh peridotites, resulting from Ca addition during seawater

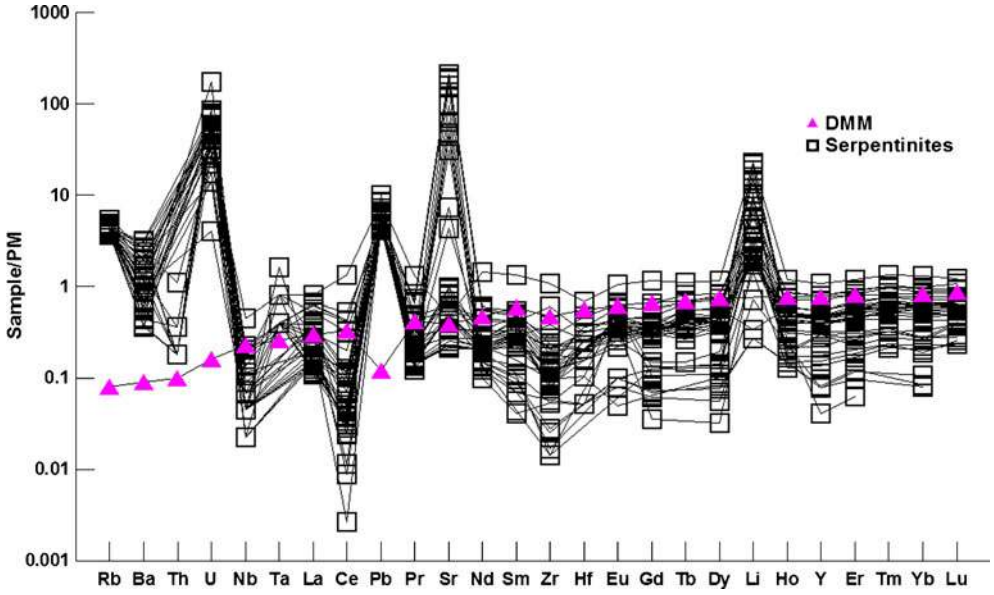

Figure 8. PM-normalised trace element patterns of serpentinites. PM data are from McDonough and Sun (1995); DMM data are from Workman and Hart (2005).

alteration. In addition, the Rb, Ba, U, Pb, Sr and Li positive anomalies, shown in figure 8, are most likely attributed to seawater–rock interactions. Seawater can interact directly with peridotite exposed on the seafloor (Kelley *et al.* 2005a), and the reaction of seawater with peridotite causes serpentinization (Janecky and Seyfried 1986). Seawater infiltration facilitates serpentinization processes, including the hydration of olivine and orthopyroxene to variants of phyllosilicate serpentine (Schroeder *et al.* 2002). Ba and U enrichments in the serpentinite samples from the super slow-spreading SWIR near 65°E are mostly likely related to low-temperature alteration (Augustin *et al.* 2008). During the peridotite–fluid interaction stage, Sr was probably incorporated into the Ca-rich phases, such as carbonate, tremolite and diopside (Scambelluri *et al.* 2001), while U and Pb were probably bound in the carbonate and sulfides, respectively (Kelley *et al.* 2005b). Li was generally incorporated into chlorite and amphiboles (Bebout *et al.* 2007).

Figure 10 illustrates the features of the Th/Nb and La/Nb ratios revealed by comparison with other representative origins. Some serpentinites plot close to the continental crust field, suggesting

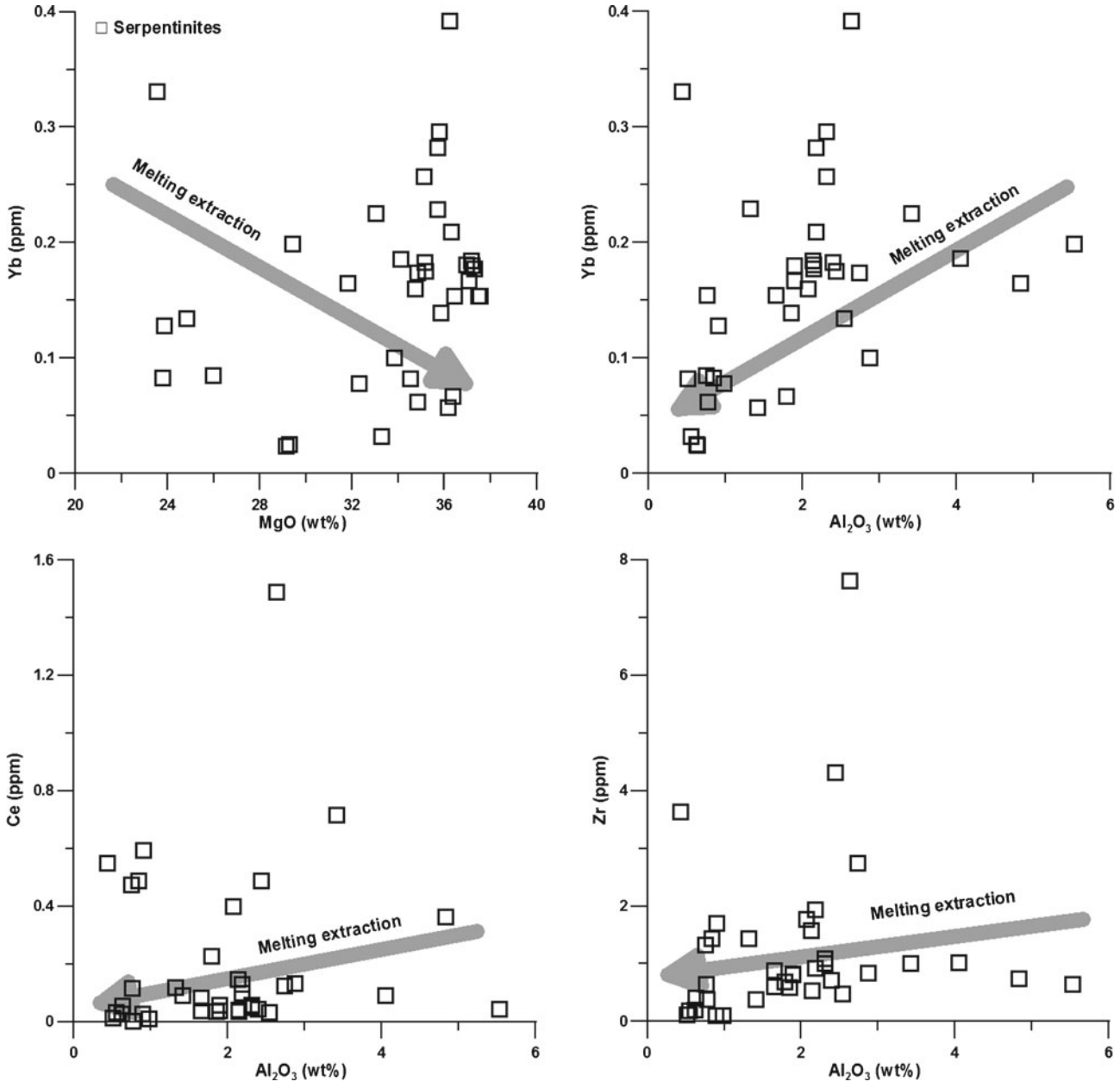

Figure 9. Bulk rock major element and trace element correlation plots of serpentinites. (**a**) The variation of Yb with bulk rock MgO content is consistent with the different degrees of melting and melt extraction. (**b**), (**c**), (**d**) Yb, Ce and Zr (respectively) correlate negatively with Al_2O_3, consistent with the partial melting trend.

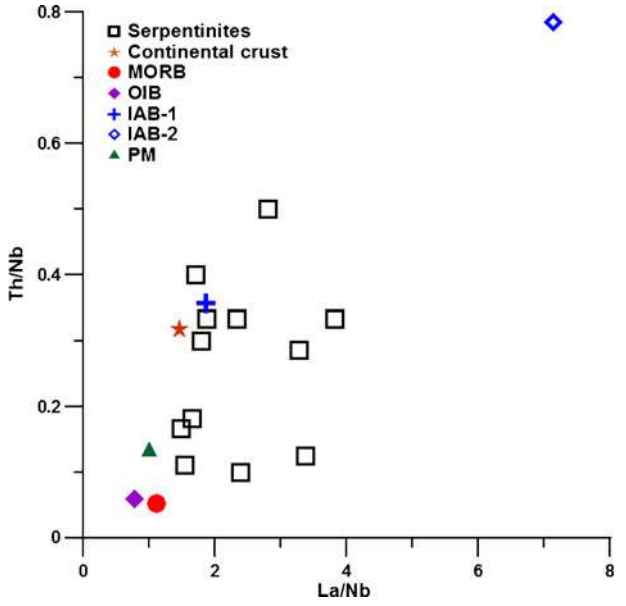

Figure 10. Plot of Th/Nb *vs.* La/Nb for the serpentinites. Continental crust and mid-ocean ridge basalt (MORB), ocean island basalt (OIB), island arc tholeiite high-Al basalt (IAB-1), island arc calc-alkali basalt (IAB-2) and PM data are from Hofmann (1988), Donnelly *et al.* (2004), Sun (1980), McDonough and Sun (1995), respectively.

that continental crust was involved in the oceanic crust transition and contributed to the creation of the new oceanic crust. Other serpentinites with relatively high Th/Nb ratios plot between the MORB and arc basalts, implying that seawater–rock reactions could have caused high Th/Nb ratios, because seawater-related fluid prefers fluid-mobile elements such as Rb, Sr and Th, rather than more strongly bound (less mobile) elements such as Nb. The high Ce/Pb value (∼14000) in the oceanic crust was in contrast to the distinctly low Ce/Pb value (∼4) in the continental crust (Taylor and McLennan 1985). The Ce/Pb ratios of some serpentinites were significantly lower than that of the continental crust, slightly higher than that (Ce/Pb = 0.01) of PM, and similar to that (Ce/Pb = 0.04) of seawater (Turekian 1968), also implying that some of the serpentinites have undergone seawater alteration.

5. Conclusions

- The abyssal peridotites from the super slow-spreading SWIR near 65°E have been altered by seawater, and transformed into the serpentinites with lizardite, chlorite, carbonate, magnetite, talc and relict olivine and pyroxene.
- The serpentinites still contain information about their magma source and about seawater alteration in both their primary and secondary minerals. The serpentinites exhibit evidence of talc reduction or decompression during seawater–rock interaction.

The trace element composition of the serpentinites reveals depletion in most incompatible elements, similarly to that of DMM indicating that the SWIR peridotites originated from the depleted mantle source magma and experienced partial melting. Rb, Ba, U, Pb, Sr and Li anomalies, and the Ce/Pb ratio of the serpentinites, show that these serpentinites have undergone strong seawater alteration.

Acknowledgements

Authors would like to thank the crews of the DY105-17A cruise for the help to collect samples. The authors gratefully acknowledge Shanke Liu (IGGCAS), Dingshuai Xue (IGGCAS) and He Li (IGGCAS) for technical assistance with XRD and XRF analyses. We are most grateful for the detailed and constructive comments and suggestions provided by the anonymous reviewer and the Associate Editor Dr. Somnath Dasgupta, which significantly improved the content of this paper. They also like to thank International Science Editing for checking our English. This work was supported by National Natural Science Foundation of China (Grant No. 40830849, 40976027), Shandong Province Natural Science Foundation of China for Distinguished Young Scholars (Grant No. JQ200913), and National Special Fund for the Twelfth Five Year Plan of COMRA (Grant No. DY125-12-R-02 and Grant No. DY125-11-R-05).

References

Alt J C and Shanks W C III 1998 Sulfur in serpentinized oceanic peridotites: Serpentinization processes and microbial sulfate reduction; *J. Geophys. Res.* **103** 9917–9929.

Alt J C and Shanks W C III 2003 Serpentinization of abyssal peridotites from the MARK area, Mid-Atlantic Ridge: Sulfur geochemistry and reaction modeling; *Geochim. Cosmochim. Acta* **67** 641–653.

Asimow P D 1999 A model that reconciles major- and trace-element data from abyssal peridotites; *Earth Planet. Sci. Lett.* **169** 303–319.

Augustin N, Lackschewitz K S, Kuhn T and Devey C W 2008 Mineralogical and chemical mass changes in mafic and ultramafic rocks from the Logatchev hydrothermal field (MAR 15°N); *Marine Geol.* **256** 18–29.

Aumento F and Loubat H 1971 The Mid-Atlantic Ridge near 45°N. XVI. Serpentinized ultramafic intrusions; *Canadian J. Earth Sci.* **8** 631–663.

Bach W, Garrido C J, Paulick H, Harvey J and Rosner M 2004 Seawater–peridotite interactions: First insights from ODP Leg 209, MAR 15°N; *Geochem. Geophys. Geosyst.* **5(9)** Q09F26, doi: 10.1029/2004GC00 0744.

Baker M B and Beckett J R 1999 The origin of abyssal peridotite: A reinterpretation of constraints based on primary bulk composition; *Earth Planet. Sci. Lett.* **171** 49–61.

Baker M B and Stolper E M 1994 Determining the composition of high-pressure mantle melts using diamond aggregates; *Geochim. Cosmochim. Acta* **58** 2811–2827.

Bebout G E, Bebout A E and Graham C M 2007 Cycling of B, Li, and LILE (K, Cs, Rb, Ba, Sr) into subduction zones: SIMS evidence from micas in high-P/T metasedimentary rocks; *Chem. Geol.* **239** 284–304.

Bodinier J L 1988 Geochemistry and petrogenesis of the Lanzo peridotite body, western Alps; *Tectonophys.* **149** 67–68.

Bodinier J L, Dupuy C and Dostal J 1988 Geochemistry and petrogenesis of Eastern Pyrenean peridotites; *Geochim. Cosmochim. Acta* **52** 2893–2907.

Bonatti E, Lawrence J R and Morandi N 1984 Serpentinization of oceanic peridotites: Temperature dependence of mineralogy and boron content; *Earth Planet. Sci. Lett.* **70** 88–94.

Boschi C, Dini A, Früh-Green G L and Kelley D S 2008 Isotopic and element exchange during serpentinization at the Atlantis massif (MAR 30°N): Insights from B and Sr isotope data; *Geochim. Cosmochim. Acta* **72** 1801–1823.

Bown J W and White R S 1994 Variation with spreading rate of oceanic crustal thickness and geochemistry; *Earth Planet. Sci. Lett.* **121** 435–449.

Brunelli D, Seyler M, Cipriani A, Ottolini L and Bonatti E 2006 Discontinuous melt extraction and weak refertilization of mantle peridotites at the Vema lithospheric section (Mid-Atlantic Ridge); *J. Petrol.* **47** 745–771.

Cannat M 1996 How thick is the magmatic crust at slow spreading oceanic ridges?; *J. Geophys. Res.* **101** 2847–2857.

Cannat M, Mével C, Maia M, Deplus C, Durand C, Gente P, Agrinier P, Belarouchi A, Dubuisson G, Humler E and Reynolds J 1995 Thin crust, ultramafic exposures, and rugged faulting patterns at the Mid-Atlantic Ridge (22°–24°N); *Geology* **23** 49–52.

Cannat M, Sauter D, Mendel V, Ruellan E, Okino K, Escartin J, Combier V and Baala M 2006 Modes of seafloor generation at a melt-poor ultraslow-spreading ridge; *Geology* **34** 605–608.

Charlou J L, Fouquet Y, Bougault H, Donval J P, Etoubleau J, Jean-Baptiste J, Dapoigny A, Appriou P and Rona P A 1998 Intense CH_4 plumes generated by serpentinization of ultramafic rocks at the intersection of the 15°20′N fracture zone and the Mid-Atlantic Ridge; *Geochim. Cosmochim. Acta* **62** 2323–2333.

Christensen N 1972 The abundance of serpentinites in the ocean crust; *J. Geol.* **80** 709–719.

Class C and le Roex A P 2008 Ce anomalies in Gough island lavas – trace element characteristics of a recycled sediment component; *Earth Planet. Sci. Lett.* **265** 475–486.

Dick H J B, Fisher R L and Bryan W B 1984 Mineralogic variability of the uppermost mantle along mid-ocean ridges; *Earth Planet. Sci. Lett.* **69** 88–106.

Donnelly K E, Goldstein S L, Langmuir C H and Spiegelman M 2004 Origin of enriched ocean ridge basalts and implications for mantle dynamics; *Earth Planet. Sci. Lett.* **226** 347–366.

Douville E, Charlou J L, Oelkers E H, Bienvenu P, Jove Colon C F, Donval J P, Fouquet Y, Prieur D and Appriou P 2002 The rainbow vent fluids (36°14′N, MAR): The influence of ultramafic rocks and phase separation on trace metal content in Mid-Atlantic Ridge hydrothermal fluids; *Chem. Geol.* **184** 37–48.

Elthon D 1992 Chemical trends in abyssal peridotites: Refertilization of depleted suboceanic mantle; *J. Geophys. Res.* **97** 9015–9025.

Engel C G and Fisher R L 1975 Granitic to ultramafic rock complexes of the Indian Ocean Ridge System, western Indian Ocean; *Geol. Soc. Am. Bull.* **86** 1553–1578.

Escartin J, Hirth G and Evans B 1997 Nondilatant brittle deformation of serpentinites: Implications for Mohr–Coulomb theory and the strength of faults; *J. Geophys. Res.* **102** 2897–2913.

Escartin J, Hirth G and Evans B 2001 Strength of slightly serpentinized peridotites: Implications for the tectonics of oceanic lithosphere; *Geology* **29** 1023–1026.

Fox P J, Schreiber E, Rowlett H and McCamy N 1976 The geology of the Oceanographer fracture zone: A model for fracture zones; *J. Geophys. Res.* **81** 4117–4128.

Fruh-Green G L, Kelley D S, Bernasconi S M, Karson J A, Ludwig K A, Butterfield D A, Boschi C and Proskurowski G 2003 30,000 years of hydrothermal activity at the Lost City Vent Field; *Science* **301** 495–498.

Godard M, Lagabrielle Y, Alard O and Harvey J 2008 Geochemistry of the highly depleted peridotites drilled at ODP Sites 127 and 1274 (Fifteen–Twenty Fracture Zone, Mid-Atlantic Ridge): Implications for mantle dynamics beneath a slow spreading ridge; *Earth Planet. Sci. Lett.* **267** 410–425.

Hajash A and Chandler G W 1981 An experimental investigation of high-temperature interactions between rhyolite, andesite, basalt and peridotite. *Contrib. Mineral. Petrol.* **78** 240–254.

Hamlyn P R and Bonatti E 1980 Petrology of mantle-derived ultramafics from the Owen Fracture Zone, Northwest Indian Ocean: Implications for the nature of the oceanic upper mantle; *Earth Planet. Sci. Lett.* **48** 65–79.

Harvey J, Gannoun A, Burton K W, Rogers N W, Alard O and Parkinson I J 2006 Ancient melt extraction from the oceanic upper mantle revealed by Re-Os isotopes in abyssal peridotites from the Mid-Atlantic ridge; *Earth Planet. Sci. Lett.* **244** 606–621.

Hellebrand E, Snow J E, Hoppe P and Hofmann A W 2002 Garnet-field melting and late-stage refertilization in 'residual' abyssal peridotites from the Central Indian Ridge; *J. Petrol.* **43** 2305–2338.

Hilairet N, Reynard B, Wang Y, Daniel I, Merkel S, Nishiyama N and Petigirard S 2008 High-pressure creep of serpentinite, interseismic deformation, and initiation of subduction; *Science* **318** 1910–1913.

Hirose T, Bystricky M, Kunze K and Stunitz H 2006 Semi-brittle flow during dehydration of lizardite–chrysotile serpentinite deformed in torsion: Implications for the rheology of oceanic lithosphere; *Earth Planet. Sci. Lett.* **249** 484–493.

Hofmann A W 1988 Chemical differentiation of the earth: The relationship between mantle, continental crust and oceanic crust; *Earth Planet. Sci. Lett.* **90** 297–314.

Horita J and Berndt M E 1999 Abiogenic methane formation and isotope fractionation under hydrothermal conditions; *Science* **285** 1055–1057.

Janecky D R and Seyfried W E Jr 1986 Hydrothermal serpentinization of peridotite within the oceanic crust: Experimental investigations of mineralogy and major element chemistry; *Geochim. Cosmochim. Acta* **50** 1357–1378.

Johnson K T M, Dick H J B and Shimizu N 1990 Melting in the oceanic upper mantle: An ion microprobe study of diopsides in abyssal peridotites; *J. Geophys. Res.* **95** 2661–2678.

Kelley D S, Karson J A, Blackman D K, Früh-Green G L, Butterfield D A, Lilley M D, Olson E J, Schrenk M O, Roe K K, Lebon G T and Rivizzigno P and AT3-60 Shipboard Party 2001 An off-axis hydrothermal vent field near the Mid-Atlantic Ridge at 30°N; *Nature* **412** 145–149.

Kelley D S, Karson J A, Früh-Green G L, Yoerger D R, Shank T M, Butterfield D A, Hayes J M, Schrenk M O, Olson E J, Proskurowski G, Jakuba M, Bradley A, Larson B, Ludwig K, Glickson D, Buckman K, Bradley A S, Brazelton W J, Roe K, Elend M J, Delacour A, Bernasconi S M, Lilley M D, Baross J A, Summons R E and Sylva S P 2005a A serpentinite-hosted ecosystem: The lost city hydrothermal field; *Science* **307** 1428–1434.

Kelley K A, Plank T T, Farr L, Ludden J and Staudigel H 2005b Subduction cycling of U, Th, and Pb; *Earth Planet. Sci. Lett.* **234** 369–383.

Klinkhammer G, Elderfield H, Edmond J and Mitra A 1994 Geochemical implications of rare earth element patterns in hydrothermal fluids from mid-ocean ridges; *Geochim. Cosmochim. Acta* **58(23)** 5105–5113.

Luo Y, Gao S, Yuan H L, Liu X M, Deltlef G, Jin Z M and Sun M 2004 Ce anomaly in minerals of eclogite and garnet pyroxenite from Dabie-Sulu ultra-high pressure metamorphic belt: Tracking subducted sediment formed under oxidizing conditions. *Science in China; Series D: Earth Sciences* **34** 920–930.

McDonough W F and Sun S S 1995 The composition of the Earth; *Chem. Geol.* **120** 223–253.

Mendel V and Sauter D 1997 Seamount volcanism at the super slow-spreading southwest Indian Ridge between 57°E and 70°E; *Geology* **25** 99–102.

Mendel V, Sauter D, Parson L and Vanney J 1997 Segmentation and morphotectonic variations along a super slow-spreading center: The southwest Indian Ridge (57°–70°E); *Marine Geophys. Res.* **19** 503–531.

Mével C 2003 Serpentinisation of abyssal peridotite at mid ocean ridges; *Comptes Rendus Geosci.* **335** 825–852.

Morishita T, Hara K, Nakamura K, Sawaguchi T, Tamura A, Arai S, Okino K, Takai K and Kumagai H 2009 Igneous, alteration and exhumation processes recorded in abyssal peridotites and related fault rocks from an oceanic core complex along the Central Indian Ridge; *J. Petrol.* **50** 1299–1325.

Niu Y 1997 Mantle melting and melt extraction processes beneath ocean ridges: Evidence from abyssal peridotites; *J. Petrol.* **38** 1047–1074.

Niu Y 2004 Bulk-rock major and trace element compositions of abyssal peridotites: Implications for mantle melting, melt extraction and post-melting processes beneath mid-ocean ridge; *J. Petrol.* **45** 2423–2458.

Niu Y and Hekinian R 1997 Basaltic liquids and harzburgitic residues in the Garrett Transform: A case study at fast-spreading ridges; *Earth Planet. Sci. Lett.* **146** 243–258.

Niu Y, Langmuir C H and Kinzler R J 1997 The origin of abyssal peridotites: A new perspective; *Earth Planet. Sci. Lett.* **152** 251–265.

Parkinson I J, Pearce J A, Thirlwall M F, Johnson K T M and Ingram G 1992 28 Trace element geochemistry of peridotites from the Izu–Bonin–Mariana forearc, Leg 125. Proceedings of the Ocean Drilling Program; *Scientific Results* **125** 487–506.

Patriat Ph and Parson L 1989 A survey of the Indian Ocean Triple Junction Trace within the Antarctic Plate. Implications for the junction evolution since 15 Ma; *Marine Geophys. Res.* **11** 89–100.

Patriat Ph, Sauter D, Munschy M and Parson L 1997 A survey of the Southwest Indian Ridge Axis between Atlantis II Fracture Zone and the Indian Ocean Triple Junction: Regional setting and large scale segmentation; *Marine Geophys. Res.* **19** 457–480.

Paulick H, Bach W, Godard M, DeHoog J C M, Suhr G and Harvey J 2006 Geochemistry of abyssal peridotites (Mid-Atlantic Ridge, 15°20′N, ODP Leg 209): Implications for fluid/rock interaction in slow spreading environments; *Chem. Geol.* **234** 179–210.

Pereira M D, Shaw D M and Acosta A 2003 Mobile trace elements and fluid-dominated processes in the Ronda peridotite, southern Spain; *The Canadian Mineralogist* **41** 617–625.

Prinz M, Keil K, Green J A, Reid A M, Bonatti E and Honnorez J 1976 Ultramafic and mafic dredge samples from the equatorial Mid-Atlantic Ridge and fracture zones; *J. Geophys. Res.* **81** 4087–4103.

Rampone E, Romairone A and Hofmann A W 2004 Contrasting bulk and mineral chemistry in depleted mantle peridotites: Evidence for reactive porous flow; *Earth Planet. Sci. Lett.* **218** 491–506.

Ray D, Banerjee R, Iyer S D and Mukhopadhyay S 2008 A new report of serpentinites from Northern Central Indian Ridge (at 6°S) – an implication for hydrothermal activity; *Acta Geologica Sinica* **82(6)** 1213–1222.

Robinson C J, Bickle M J, Minshull T A, White R S and Nichols A R L 2001 Low degree melting under the Southwest Indian Ridge: The roles of mantle temperature, conductive cooling and wet melting; *Earth Planet. Sci. Lett.* **188** 383–398.

Savov I P, Guggino S, Ryan J G, Fryer P and Mottl M J 2005 4. Geochemistry of serpentinite muds and metamorphic rocks from the Mariana forearc, ODP Sites 1200 and 778–779, South Chamorro and Conical seamounts; In: Proceedings of the Ocean Drilling Program (eds) Shinohara M, Salisbury M H and Richter C, *Scientific Results* **195** 1–49.

Scambelluri M, Rampone E and Piccardo G B 2001 Fluid and element cycling in subducted serpentinite: A trace element study of the Erro-Tobbio high-pressure ultramafites (Western Alps, NW Italy); *J. Petrol.* **4** 55–67.

Schroeder T, John B and Frost B R 2002 Geologic implications of seawater circulation through peridotite exposed at slow-spreading mid-ocean ridges; *Geology* **30** 367–370.

Seyler M, Loarnd J-P, Dick H J B and Drouin M 2007 Pervasive melt percolation reactions in ultra-depleted refractory harzburgites at the Mid-Atlantic Ridge, 15°20′N: ODP Hole 1274A; *Contrib. Mineral. Petrol.* **153** 303–319.

Snow J E and Dick H J B 1995 Pervasive magnesium loss by marine weathering of peridotite; *Geochim. Cosmochim. Acta* **59** 4219–4235.

Sun S-S 1980 Lead isotopic study of young volcanic rocks from Mid-Ocean ridges, Ocean Islands and Island Arcs; Philosophical Transactions of the Royal Society of London, Series A, *Mathematical and Physical Sciences* **297(1431)** 409–445.

Takai K, Nakamura K, Suzuki K, Inagaki F, Nealson K H and Kumagai H 2006 Ultramafics–Hydrothermalism–Hydrogenesis–HyperSLiME (UltraH3) linkage: A key insight into early microbial ecosystem in the Archean deep-sea hydrothermal systems; *Paleontological Res.* **10** 269–282.

Tamura A, Arai S, Ishimaru S and Andal E S 2008 Petrology and geochemistry of peridotites from IODP Site U1309 at Atlantis Massif, MAR 30°N: micro- and macro-scale melt penetrations into peridotites; *Contrib. Mineral. Petrol.* **155** 491–509.

Taylor S R and McLennan S M 1985 The continental crust: Its composition and evolution; Blackwell, Oxford, 312p.

Thompson G and Melson W G 1970 Boron contents of serpentinites and metabasalts in the oceanic crust: Implications for the boron cycle in the oceans; *Earth Planet. Sci. Lett.* **8** 61–65.

Turekian K K 1968 *Oceans*; Prentice-Hall, Engelwood Cliffs, NJ, 120p.

Walter M J 1998 Melting of garnet peridotite and the origin of komatiite and depleted lithosphere; *J. Petrol.* **39** 29–60.

Wenner D B and Taylor H P 1973 Oxygen and hydrogen isotope studies of serpentinisation of ultramafic rocks; *Am. J. Sci.* **273** 207–239.

White R S, Mckenzie D P and O'Nions R K 1992 Oceanic crustal thickness from seismic measurements and rare earth element inversions; *J. Geophys. Res.* **97** 19,683–19,715.

White R S, Minshull T A, Bickle M J and Robinson C J 2001 Melt generation at very slow-spreading oceanic ridges: Constraints from geochemical and geophysical data; *J. Petrol.* **42** 1171–1196.

Whitmarsh R B, Manatschal G and Minshull T A 2001 Evolution of magma-poor continental margins from rifting to seafloor spreading; *Nature* **413** 150–154.

Wicks F J and Whittaker E J W 1977 Serpentine textures and serpentinisation; *Canadian Mineralogist* **15** 459–488.

Workman R K and Hart S R 2005 Major and trace element composition of the depleted MORB mantle (DMM); *Earth Planet. Sci. Lett.* **231** 53–72.

MS received 2 June 2011; revised 6 May 2012; accepted 18 May 2012